

Distribution-Free Selection of Low-Risk Oncology Patients for Survival Beyond a Time Horizon

Matteo Sesia^{*1} and Vladimir Svetnik²

¹Departments of Data Sciences and Operations, and of Computer Science, University of Southern California, California, USA

²Merck & Co., New Jersey, USA

Abstract

We study the problem of selecting a subset of patients who are unlikely to experience an adverse event within a fixed time horizon by calibrating a screening rule based on a black-box survival model. We consider two complementary, distribution-free frameworks for this task. The first extends classical calibration ideas—estimating the event rate among selected patients using a hold-out dataset—by integrating them with the Learn–Then–Test (LTT) framework, yielding high-probability guarantees for data-adaptively tuned screening rules. The second takes a different perspective by reformulating screening as a hypothesis testing problem on future patient outcomes, enabling false discovery rate (FDR) control via the Benjamini–Hochberg procedure applied to selective conformal p-values, and providing guarantees in expectation. We clarify the theoretical relationship between these approaches, explain how both can be adapted to right-censored time-to-event data via inverse probability of censoring weighting, and compare them empirically using simulations and oncology data from the Flatiron Health Research Database. Our results reveal a trade-off between efficiency and strength of guarantees: FDR-based screening is typically more powerful, while LTT-based calibration is more conservative but offers stronger guarantees. We also provide practical guidance on implementation and tuning.

1 Introduction

1.1 Background and Motivation

A common statistical question in medicine is to how to identify a subset of patients who are sufficiently unlikely to experience an adverse event within a fixed time horizon. This problem has many applications, including determining eligibility for less intensive management strategies such as active surveillance instead of surgery, and optimizing the allocation of limited clinical resources toward patients most likely to benefit. From a statistical perspective, this can be viewed as a large-scale testing problem: among many candidates, the goal is to select as many as possible of those who are truly low-risk, while controlling the rate of type-I errors—patients who are selected but nonetheless experience the event within the horizon of interest. In practice, this task is further complicated by right-censoring, as follow-up may end before the event occurs for many patients, leaving their event status by the time horizon of interest unobserved.

As a concrete example arising from oncology care, consider a phase II de-escalation study that aims to enroll only patients who are sufficiently low risk, with a protocol target of no more than

^{*}CONTACT Matteo Sesia. Email: sesia@marshall.usc.edu

10% event probability within 3 months among participants. This means that approximately 90% of enrolled patients should remain event-free for at least 3 months. Proper calibration of the screening rule is essential and requires balancing competing considerations: an overly liberal rule may admit too many high-risk patients, raising safety concerns or prompting early study termination, whereas an overly conservative rule may exclude many eligible patients, resulting in missed opportunities to improve patient well-being and make scientific findings.

In modern clinical practice, patient screening is typically data-driven and guided by survival probabilities estimated from predictive models that leverage rich demographic information and detailed clinical histories. Classical approaches include exponential or Weibull models and the semi-parametric Cox proportional hazards model (Cox, 1972), while in large-scale, high-dimensional settings more flexible machine-learning methods (Bertsimas and Wiberg, 2020)—including random survival forests (Ishwaran et al., 2008), deep neural networks (Katzman et al., 2018), and gradient-boosting models (Barnwal et al., 2022)—often provide more accurate risk stratification.

Yet, all such models have limitations: classical survival models rely on assumptions that may be difficult to validate (e.g., parametric forms or proportional hazards), whereas machine-learning approaches typically prioritize point predictions over principled uncertainty estimation. As a result, it is natural to treat the predictive model itself as a “black box” and seek statistical guarantees directly at the level of the downstream screening rule, which selects patients whose estimated survival probabilities exceed a threshold that needs to be *calibrated* after the model has been trained.

A standard way to *evaluate* the event rate among patients selected by a given screening rule is to apply it to an independent hold-out dataset. Under right-censoring, this is commonly done using inverse probability of censoring weighting (IPCW), which provides consistent estimates of time-dependent event rates under standard assumptions on the censoring mechanism (Robins and Rotnitzky, 1992; Robins, 1993). IPCW-based estimators can further be paired with asymptotic or resampling-based inference techniques to construct confidence intervals for the corresponding event rate. When evaluating a fixed screening rule, pointwise inference over the threshold is sufficient, although more conservative simultaneous confidence bands can also be constructed.

The main challenge is that screening rules are typically tuned by evaluating performance across multiple candidate thresholds and choosing the one that maximizes yield subject to an acceptable event rate. Pointwise confidence intervals do not account for this data-dependent selection and therefore fail to provide valid guarantees for the chosen rule, while uniform confidence bands, although valid, are often overly conservative and lead to inefficient screening. These limitations motivate the need for methods that can carefully account for data-dependent tuning while providing meaningful statistical guarantees, all while accommodating right-censoring in the data.

1.2 Contributions

This paper makes three main contributions addressing the challenge described above. First, we show how to rigorously and efficiently calibrate screening rules under right-censoring using IPCW estimates of the event rate among selected patients. Our approach applies fixed-sequence testing (Bauer, 1991) via the Learn–Then–Test (LTT) framework (Angelopoulos et al., 2024a, 2025) to pointwise IPCW risk bounds, yielding high-probability guarantees for data-driven screening rules. These guarantees are comparable in strength to those obtained from uniform confidence bounds, but are achieved less conservatively, resulting in selection yields close to those attainable through naive pointwise calibration. To the best of our knowledge, this represents the first application of the LTT framework with right-censored time-to-event data.

Second, we study an alternative calibration strategy based on false discovery rate (FDR) con-

trol. We explicitly formulate the screening problem as a hypothesis testing problem on future patient event times, construct “selective” conformal p-values (Jin and Candès, 2023) using IPCW to account for censoring, and then apply the classical Benjamini–Hochberg procedure (Benjamini and Hochberg, 1995). This yields control of the event fraction among selected patients in expectation, rather than with high probability. One practical advantage of the FDR-based approach is that it does not require pre-specification of a confidence level, which we show can involve difficult trade-offs in practice. While this methodology was recently proposed by Sesia and Svetnik (2025b), we refine its implementation by introducing a key tuning parameter that substantially increase selection yield while preserving theoretical guarantees.

Third, we provide a direct theoretical and empirical comparison of high-probability risk control and FDR-based calibration approaches. Although these methods rely on different notions of error control, they essentially address the same practical calibration objective and can be meaningfully compared. We clarify the interpretation of their guarantees, identify regimes in which their behavior diverges, and characterize the resulting trade-offs between conservativeness and efficiency. A key theoretical contribution is Theorem 2, which establishes an explicit relationship between the FDR and the selected-set event rate, formalizing how the two concepts diverge only when selection events are very rare. We further compare both approaches empirically against classical calibration strategies based on pointwise and uniform IPCW-based confidence intervals (Park and Wei, 2003; Zheng et al., 2008, 2010; Fleming and Harrington, 2013).

Table 1: Summary of low-risk patient screening methods and benchmarks compared in this paper. The first four methods are statistically principled calibration procedures that use inverse probability of censoring weighting (IPCW) and are studied both theoretically and empirically. They differ in the type of calibration guarantee they provide as well as in whether they operate from an inductive or cohort-adaptive (transductive) perspective. The last two rows correspond to reference benchmarks included in the empirical comparison: a model-based baseline that treats predicted survival probabilities as exact, and an oracle benchmark that assumes access to the true population-level survival function.

Method	Calibration	Perspective	Yield	Where
HP–Pointwise	Heuristic	Inductive	High	Section 3.2
HP–Uniform	High-probability	Inductive	Low	Section 3.3
HP–LTT	High-probability	Inductive	Medium	Section 3.4
FDR–Conformal	In expectation	Transductive	High	Section 4
Model-based baseline	None	Inductive	High	Section 5
Oracle benchmark	Exact	Inductive	Optimal	Section 5

1.3 Related Works

This paper builds upon a rich and diverse literature on multiple testing (Benjamini and Hochberg, 1995; Storey et al., 2004), IPCW for right-censored time-to-event data (Robins and Rotnitzky, 1992; Robins, 1993; Vock et al., 2016), distribution-free risk control via the LTT framework (Angelopoulos et al., 2024a, 2025), and conformal prediction (Vovk et al., 2005; Angelopoulos and Bates, 2023; Angelopoulos et al., 2024b). Our work integrates ideas from these largely distinct lines of research.

The LTT approach adopts an *estimation-oriented* perspective, leading to *high-probability* guarantees on the realized risk of the selected subset. This perspective is closely aligned with standard

calibration practices, which typically rely on IPCW estimates of event rates among selected patients as a function of the screening threshold parameter. Despite this natural connection, and to the best of our knowledge, the LTT framework has seen limited use in the analysis of censored time-to-event data. This is somewhat surprising given its generality and ease of implementation.

Conformal prediction offers a complementary approach from a *predictive inference* perspective, focusing on guarantees for future individual observations rather than estimation of population-level risks. It has been the subject of substantial recent research and has seen growing use in medical applications (Vazquez and Facelli, 2022; Olsson et al., 2022), including oncology (Bergquist et al., 2022). In time-to-event settings, conformal inference methods have been used to construct prediction intervals for event times under various censoring regimes (Candès et al., 2023; Gui et al., 2024; Qin et al., 2025; Farina et al., 2025; Davidov et al., 2025; Sesia and Svetnik, 2025a). In this paper, we instead apply conformal prediction to calibrate cohort screening rules, using selective conformal p-values (Jin and Candès, 2023) combined with the Benjamini–Hochberg procedure (Benjamini and Hochberg, 1995) and adopting the IPCW-based approach of Sesia and Svetnik (2025b) to account for right-censoring.

The problem studied in this paper is related to, but distinct from, time-dependent receiver operating characteristic (ROC) analysis, which focuses on assessing how well a prognostic score ranks patients according to their risk of experiencing an event by a given time horizon (Heagerty et al., 2000; Heagerty and Zheng, 2005; Blanche and Blanche, 2013; Yuan et al., 2018). Discrimination metrics such as the area under the curve quantify ranking accuracy but do not ensure that any specific decision threshold yields an acceptable event rate among patients classified as low or high risk. In contrast, clinical screening decisions depend on *calibration at the operating point*—that is, ensuring that the event rate among selected (or unselected) patients meets a predefined target. This paper addresses the calibration problem directly.

2 Preliminaries

2.1 Notation, Data, and Main Assumptions

For each individual indexed by $i \in \mathbb{N}$, let $X_i \in \mathcal{X} \subseteq \mathbb{R}^d$ denote a vector of d covariates (possibly high-dimensional), $T_i > 0$ the event time of interest, and $C_i > 0$ the censoring time, after which the individual is no longer observed. Each subject is thus represented by the triplet (X_i, T_i, C_i) . We assume that individuals are independent and identically distributed (i.i.d.) samples from an unknown underlying population. When the index is unimportant, we write (X, T, C) to denote a generic random draw from this population.

Because event and censoring times are not always jointly observable, we consider a right-censored data set. Specifically, for each individual in the available data we observe only the covariates X_i together with

$$(E_i, \tilde{T}_i) := (\mathbb{I}(T_i < C_i), \min(T_i, C_i)),$$

where $E_i \in \{0, 1\}$ indicates whether the event occurred before censoring and \tilde{T}_i denotes the observed (possibly censored) time. We adopt the standard assumption of independent censoring given covariates, namely that $T \perp C \mid X$, which is necessary to enable consistent inference from right-censored data.

Let $S(t \mid x)$ and $G(t \mid x)$ respectively denote the conditional survival and censoring functions at the population level:

$$S(t \mid x) := \mathbb{P}(T > t \mid X = x), \quad G(t \mid x) := \mathbb{P}(C \geq t \mid X = x),$$

both of which are unknown quantities. We assume access to estimates \hat{S} and \hat{G} , obtained from “black box” survival and censoring models, respectively. Accordingly,

$$\hat{S}(t | x) \approx \hat{\mathbb{P}}(T > t | X = x), \quad \hat{G}(t | x) \approx \hat{\mathbb{P}}(C \geq t | X = x),$$

where the symbol \approx denotes an aspirational approximation whose accuracy may vary in practice. These models may be parametric, semi-parametric, or based on complex machine-learning algorithms. In practice, the censoring model is typically trained analogously to the survival model, but with the event indicators reversed.

The fitted survival model is used to compute covariate-based scores $\hat{z}(x) \in [0, 1]$ that rank patients according to their estimated likelihood of surviving beyond a fixed time horizon $t_0 > 0$. The most direct choice is

$$\hat{z}(x) = \hat{S}(t_0 | x), \tag{1}$$

although alternative constructions that leverage additional information from the full estimated survival distribution are also possible, as discussed later. The estimated censoring function \hat{G} is used for IPCW-based inference, as detailed in Section 2.3.

2.2 Problem Statement and Outline of Approaches

Recall that our goal is to confidently identify a subset of low-risk patients who are sufficiently unlikely to experience an adverse event within the time horizon t_0 . An intuitive way to formalize this problem is to consider a monotone family of screening rules indexed by a threshold parameter $\lambda \in [0, 1]$:

$$A_\lambda(x) := \mathbb{I}\{\hat{z}(x) \geq \lambda\}, \tag{2}$$

where $A_\lambda(X_i)$ is the selection indicator for subject i .

Throughout this paper, we treat the scoring function \hat{z} as fixed and focus on selecting a suitable data-driven threshold $\hat{\lambda}$ using a calibration dataset

$$\mathcal{D}_{\text{cal}} := \{(X_i, \tilde{T}_i, E_i)\}_{i=1}^n,$$

consisting of n i.i.d. right-censored observations drawn from the target population and assumed to be independent of the fitted models \hat{S} and \hat{G} . Intuitively, the calibrated screening rule defined by $\hat{\lambda}$ should select as many patients as possible while ensuring, in a statistically principled sense made precise below, that the selected patients are truly “low risk” within the specified time horizon t_0 .

Given any (possibly data dependent) screening rule $A : \mathcal{X} \rightarrow 0, 1$, we define the *selected-set risk* at time t_0 (conditional on \mathcal{D}_{cal} , on which the rule may depend) as:

$$r(A; \mathcal{D}_{\text{cal}}) := \mathbb{P}(T \leq t_0 | A(X) = 1, \mathcal{D}_{\text{cal}}); \tag{3}$$

in other words, this is the expected event rate before t_0 among selected patients. Similarly, define the expected *yield* (conditional on \mathcal{D}_{cal}) as:

$$\mu(A; \mathcal{D}_{\text{cal}}) := \mathbb{P}(A(X) = 1 | \mathcal{D}_{\text{cal}}). \tag{4}$$

The explicit dependence of r and μ on \mathcal{D}_{cal} emphasizes that both quantities are random if the selection rule depends on a data-driven threshold $\hat{\lambda}$ (e.g., $A = A_{\hat{\lambda}}$). We will sometimes suppress this dependence in notation when it is clear from context.

Given a target event rate $\alpha \in (0, 1)$, our goal is to calibrate a *data-driven* screening threshold $\hat{\lambda}$, based on the data in \mathcal{D}_{cal} , to (approximately) solve:

$$\begin{aligned} & \text{maximize}_{\lambda \in [0,1]} && \mu(A_\lambda; \mathcal{D}_{\text{cal}}) \\ & \text{subject to} && r(A_\lambda; \mathcal{D}_{\text{cal}}) \leq \alpha. \end{aligned} \tag{5}$$

In practice, both $r(A_\lambda; \mathcal{D}_{\text{cal}})$ and $\mu(A_\lambda; \mathcal{D}_{\text{cal}})$ must be estimated, and thus this stochastic optimization problem can only be solved *approximately*. The remainder of this paper discusses different solution strategies, providing different guarantees and trade-offs between conservativeness and efficiency.

In Section 3, we present methods designed to approximately solve (5) from an *inductive* perspective, allowing the solution $\hat{\lambda}$ to depend only on \mathcal{D}_{cal} and enforcing the risk constraint with high probability over the randomness in the calibration data. In Section 4, we introduce an alternative approach from a *transductive* (or *cohort-adaptive*) perspective, which additionally allows $\hat{\lambda}$ to depend on the observed covariate data from the specific cohort to which the screening rule is applied, and seeks to satisfy the risk constraint in expectation. Because both families of methods rely on IPCW to handle right-censoring in \mathcal{D}_{cal} , we first provide a brief review of IPCW.

2.3 Brief Review of Inverse Probability of Censoring Weighting

IPCW is a standard approach for mitigating possible censoring bias in time-to-event data. In our context, IPCW reweights each uncensored individual in the calibration data set by the inverse of their estimated probability of remaining uncensored up to the relevant time, $\hat{G}(\tilde{T}_i | X_i)$, thereby approximating what would have been observed in a fully followed cohort. The validity of IPCW-based inference rests on three assumptions: (i) conditional independent censoring: $T \perp\!\!\!\perp C | X$, meaning that censoring is uninformative given the covariates X ; (ii) positivity: $\inf_{x \in \mathcal{X}, 0 \leq t \leq t_0} G(t | x) > 0$, ensuring that every individual has a nonzero probability of remaining uncensored up to the time horizon of interest; (iii) consistent estimation of censoring probabilities: the fitted censoring model $\hat{G}(t | x)$, trained on an independent dataset, consistently approximates the true censoring survival function $G(t | x)$.

All methods described in this paper rely on IPCW to account for right-censoring, and therefore can only provide approximate guarantees hinging on the assumption that $\hat{G}(t | x)$ approximates $G(t | x)$ accurately. This assumption is standard and largely unavoidable in survival analysis, but it contrasts with more traditional applications of distribution-free methods in fully observed i.i.d. settings, where exact finite-sample guarantees can be obtained without assumptions on the predictive models.

3 Calibration via High-Probability Risk Control

In this section, we present methods to approximately solve the optimization problem in (5) while allowing the solution $\hat{\lambda}$ to depend only on the calibration data \mathcal{D}_{cal} , and aiming to satisfy the risk constraint with high probability. All these methods are based on constructing confidence bounds for the two key quantities— $r(A_\lambda; \mathcal{D}_{\text{cal}})$ and $\mu(A_\lambda; \mathcal{D}_{\text{cal}})$ —as functions of the screening threshold $\lambda \in [0, 1]$. We describe three increasingly refined approaches: (i) Pointwise calibration, which constructs upper confidence bounds for the risk at fixed values of λ and then selects the most liberal threshold meeting the constraint, ignoring the multiple-testing problem; (ii) Uniform calibration, which employs simultaneous confidence bounds across a grid of λ values to protect against data-dependent threshold tuning, at the cost of increased conservativeness; and (iii) Learn–then–Test

(LTT) or fixed-sequence calibration, which performs pointwise estimation sequentially over ordered thresholds, achieving a more practical balance between efficiency and robustness.

3.1 Pointwise Risk Estimation

For any fixed $\lambda \in [0, 1]$, the risk $r(A_\lambda)$ of the screening rule A_λ defined in (2), as given in (3), can be expressed independent of the calibration data \mathcal{D}_{cal} (since λ is fixed) as:

$$r(\lambda) = \frac{\theta(\lambda)}{\mu(\lambda)}, \quad \theta(\lambda) = \mathbb{E}[\mathbb{I}\{T \leq t_0\}A_\lambda(X)], \quad \mu(\lambda) = \mathbb{E}[A_\lambda(X)].$$

Two complementary IPCW estimators are available to estimate these quantities. The first, known as the event-time weighted (IPCW–ET) estimator, upweights observed events before t_0 by the inverse of the estimated probability of remaining uncensored just prior to the event time, $\hat{G}(\tilde{T}_i^- | X_i)$. Specifically, it computes:

$$\begin{aligned} \hat{r}_{\text{et}}(\lambda) &= \frac{\hat{\theta}_{\text{et}}(\lambda)}{\hat{\mu}(\lambda)}, \\ \hat{\theta}_{\text{et}}(\lambda) &= \frac{1}{n} \sum_{i=1}^n A_\lambda(X_i) \frac{\mathbb{I}(\tilde{T}_i \leq t_0, E_i = 1)}{\hat{G}(\tilde{T}_i^- | X_i)}, \\ \hat{\mu}(\lambda) &= \frac{1}{n} \sum_{i=1}^n A_\lambda(X_i). \end{aligned} \tag{6}$$

These estimates tend to exhibit lower variance when events are relatively frequent before time t_0 , since in that case $\hat{\theta}_{\text{et}}(\lambda)$ can be estimated from a larger effective sample.

When events are rarer before t_0 , an often preferred alternative is the fixed-time weighted (IPCW–FT) estimator; this upweights individuals known to be event-free at t_0 by the inverse probability of being uncensored at that time, $\hat{G}(t_0 | X_i)$. The corresponding estimators are

$$\hat{r}_{\text{ft}}(\lambda) = \frac{\hat{\theta}_{\text{ft}}(\lambda)}{\hat{\mu}(\lambda)}, \quad \hat{\theta}_{\text{ft}}(\lambda) = \hat{\mu}(\lambda) - \frac{1}{n} \sum_{i=1}^n A_\lambda(X_i) \frac{\mathbb{I}(\tilde{T}_i \geq t_0)}{\hat{G}(t_0 | X_i)}. \tag{7}$$

In this paper, we primarily adopt the IPCW–ET formulation (6), as it aligns more closely with the FDR method described in Section 4. We also follow the standard practice of applying mild winsorization to the IPCW weights (Cole and Hernán, 2008).

In addition to point estimates of $r(\lambda)$ and $\mu(\lambda)$, the calibration procedures considered in this paper require one-sided upper confidence bounds (UCBs) for $r(\lambda)$ at a prescribed significance level. Let $\delta \in (0, 1)$ denote the significance level, so that, for example, a 95% confidence bound corresponds to $\delta = 0.05$. Several approaches are available for constructing such bounds.

A classical approach that tends to work well in moderate-to-large samples is the delta-method. This approximates $\hat{r}(\lambda)$ as asymptotically Gaussian and computes its large-sample variance using a Taylor expansion, leading to an upper bound of the form

$$\text{UCB}^{\text{pt}}(\lambda; \delta) = \hat{r}(\lambda) + z_{1-\delta} \widehat{\text{SE}}(\hat{r}(\lambda)),$$

where $z_{1-\delta}$ is the $(1 - \delta)$ quantile of the standard normal distribution. We refer to Supplement Section A1.1 for additional details, including an expression for $\widehat{\text{SE}}(\hat{r}(\lambda))$. An alternative approach with similar characteristics is the nonparametric bootstrap; see Supplement Section A1.1.2.

When very few patients are selected (e.g., ≤ 10), the asymptotic approximations underlying both the delta-method and bootstrap are no longer justified, requiring instead the use of finite-sample confidence bounds. Finite-sample results have been the main focus of the distribution-free inference literature, including within the LTT framework (Angelopoulos et al., 2024a, 2025), though these estimates are often conservative. In our context, a relatively tight finite-sample upper confidence bound for $r(\lambda)$ can be derived by combining an empirical-Bernstein inequality (Maurer and Pontil, 2009) for the numerator with an exact binomial lower bound for the denominator; see Supplement Section A1.1.3 for further details.

3.2 Greedy Pointwise Calibration

Given a grid $\Lambda = \{\lambda_1, \dots, \lambda_K\}$ of K candidate thresholds between 0 and 1, the simplest calibration strategy is to compute the estimated risk $\hat{r}(\lambda)$ and a pointwise upper confidence bound for each $\lambda \in \Lambda$ with any of the methods from Section 3.1, then select

$$\hat{\lambda}_{\text{greedy}} \in \arg \max_{\lambda \in \Lambda} \{ \hat{\mu}(\lambda) : \text{UCB}^{\text{pt}}(\lambda; \delta) \leq \alpha \}, \quad (8)$$

where $\hat{\mu}(\lambda) = \frac{1}{n} \sum_{i=1}^n A_{\lambda}(X_i)$ is the observed yield. Ties, if any, are broken in favor of larger λ . Algorithm A2 in Supplement Section A1 summarizes this procedure.

A limitation of this strategy is that it offers no guarantees for the risk of the tuned screening rule, $r(\hat{\lambda}_{\text{greedy}})$. Pointwise confidence bounds are valid only for pre-specified thresholds, and searching across multiple λ values inflates the chance of selecting one whose UCB is spuriously optimistic. If K candidates are examined, the probability that at least one bound undercovers can increase from δ to as much as $1 - (1 - \delta)^K \approx K\delta$. This problem can be exacerbated by additional data-driven tuning choices—such as the IPCW formulation, degree of weight stabilization, or grid resolution.

3.3 Conservative Uniform Calibration

One way of ensuring valid inference after data-driven threshold selection is to replace the pointwise $\text{UCB}^{\text{pt}}(\lambda; \delta)$ for $r(\lambda)$ with a more conservative *uniform* upper confidence bound $\text{UCB}^{\text{unif}}(\lambda; \delta)$ satisfying:

$$\mathbb{P} \left[r(\lambda) \leq \text{UCB}^{\text{unif}}(\lambda; \delta), \forall \lambda \in \Lambda \right] \geq 1 - \delta.$$

The calibrated threshold can then be safely selected as

$$\hat{\lambda}_{\text{unif}} \in \arg \max_{\lambda \in \Lambda} \{ \hat{\mu}(\lambda) : \text{UCB}^{\text{unif}}(\lambda; \delta) \leq \alpha \},$$

which ensures $\mathbb{P}[r(\hat{\lambda}_{\text{unif}}) > \alpha] \leq \delta$; see Algorithm A3 in Supplement Section A1.3.

The simplest approach to obtain uniform confidence bounds applies the pointwise methods from Section 3.1 with a Bonferroni correction, replacing the confidence level δ with $\delta/|\Lambda|$. However, this tends to be overly conservative (especially when risk estimates are strongly correlated across nearby thresholds) leading to screening rules with needlessly low yield. A more efficient alternative is the Gaussian multiplier (perturbation) method, which constructs a joint confidence band by simulating correlated fluctuations in $\hat{r}(\lambda)$ across the grid. This accounts for dependencies between estimates and typically yields tighter bands than Bonferroni when $\hat{r}(\lambda)$ varies smoothly in λ . We refer to Supplement Section A1.3 for further details on both approaches.

3.4 Learn–Then–Test (LTT) Calibration

We now introduce a third high-probability calibration method that seeks a practical balance between the opposite extremes of the pointwise and uniform approaches presented above: the LTT procedure (Angelopoulos et al., 2024a, 2025).

Applying the estimation techniques described in Section 3.1, LTT constructs pointwise upper confidence bounds $\text{UCB}^{\text{pt}}(\lambda; \delta_*)$ for the risk $r(\lambda)$ over a grid Λ of candidate thresholds, using a confidence level δ_* defined below. To determine the calibrated threshold $\hat{\lambda}_{\text{LTT}}$, however, LTT does not search greedily over all $\lambda \in \Lambda$ as in (8). Instead, it evaluates whether $\text{UCB}^{\text{pt}}(\lambda; \delta_*) \leq \alpha$ sequentially over λ along one or more pre-specified, typically monotone paths through Λ —for instance, decreasing values of λ corresponding to increasingly liberal screening rules—and stops immediately before the first “unsafe” threshold where the risk upper confidence bound exceeds α . When multiple ($L > 1$) paths are considered, the final $\hat{\lambda}_{\text{LTT}}$ is the most liberal (i.e., smallest) among the corresponding stopping points.

This is an instance of fixed-sequence testing (Bauer, 1991), ensuring high-probability risk control without excessive conservativeness. Formally, if the risk upper bounds $\text{UCB}^{\text{pt}}(\lambda; \delta_*)$ are *pointwise* valid, then $\mathbb{P}[r(\hat{\lambda}_{\text{LTT}}) > \alpha] \leq \delta$. Intuitively, by setting $\delta_* = \delta/L$, LTT operates as if only L candidate thresholds were being tested. The Bonferroni adjustment in $\delta_* = \delta/L$ is typically mild, since a small number of well-designed paths ($L \ll |\Lambda|$) is usually sufficient to find a good calibrated threshold.

Concretely, we implement LTT using threshold paths defined as follows. We begin by fixing an *anchor* threshold $\lambda_0^{(1)} = 1 - \alpha$, motivated by the intuition that if the survival model \hat{S} is well-calibrated, then $\hat{s}(x) \approx S(t_0 | x)$, so selecting individuals with $\hat{s}(x) \geq \lambda$ should result in an event rate near $1 - \lambda$, implying $r(\lambda_0^{(1)}) \approx \alpha$. Then, we define a decreasing sequence $\lambda_0^{(1)} > \lambda_1^{(1)} > \lambda_2^{(1)} > \dots > 0$ to explore progressively more liberal thresholds. Intuitively, if the anchor is too conservative ($r(\lambda_0^{(1)}) < \alpha$), relaxing the threshold can safely increase yield. To guard against the possibility that the anchor itself may already be too liberal, we include a second decreasing path $\lambda_0^{(2)} > \lambda_1^{(2)} > \lambda_2^{(2)} > \dots \geq \lambda_0^{(1)}$ starting from a more conservative anchor, e.g., $\lambda_0^{(2)} = 1 - \alpha/2$.

For each candidate λ , we compute $\text{UCB}^{\text{pt}}(\lambda; \delta_*)$ for $r(\lambda)$ as described in Section 3.1, using $\delta_* = \delta/2$ since we consider $L = 2$ paths. In practice, we recommend using delta–method or bootstrap confidence bounds, resorting to finite–sample safeguards when the selected set is very small (e.g., ≤ 10). Along each path, the algorithm begins at the anchor and moves sequentially toward smaller λ . It stops when the upper confidence bound first exceeds the target level α , recording the last accepted value as $\hat{\lambda}_{\text{LTT}}^{(1)}$ or $\hat{\lambda}_{\text{LTT}}^{(2)}$, depending on the path. If no threshold is accepted, we set $\hat{\lambda}_{\text{LTT}}^{(l)} = 1$, corresponding to no selections. Finally, the calibrated LTT threshold is $\hat{\lambda}_{\text{LTT}} = \min\{\hat{\lambda}_{\text{LTT}}^{(1)}, \hat{\lambda}_{\text{LTT}}^{(2)}\}$. The complete procedure is summarized by Algorithm A4 in Supplement Section A1.4.

Compared to greedy pointwise and uniform calibration, LTT offers a practical middle ground between efficiency and conservativeness. It typically achieves much higher yield than uniform calibration while retaining a clear safety guarantee—something the greedy pointwise method lacks. A limitation of LTT is that it requires predefining the sequences of candidate thresholds, even though the most effective choice may depend on the data. The implementation described above, based on decreasing sequences starting from $\lambda_0^{(1)} = 1 - \alpha$ and $\lambda_0^{(2)} = 1 - \alpha/2$, performs well in many settings but may not be optimal in all cases. Another important consideration is the choice of the significance level δ , which governs a fundamental trade-off: smaller values (e.g., $\delta = 0.05$) yield stronger coverage guarantees but can reduce yield substantially, whereas larger values increase efficiency at the expense of interpretability and safety.

In the next section, we turn to a complementary framework based on conformal prediction and FDR control, which removes the need to specify a significance level δ .

4 Calibration via FDR Control and Conformal Inference

4.1 Cohort-Specific Screening Rules and Hypothesis Testing

We now turn to an alternative method for selecting low-risk patients that focuses on cohort-specific screening rules and reformulates the calibration problem using the language of hypothesis testing and FDR. The idea is to associate each patient in the target cohort with a statistic that quantifies evidence against a “null hypothesis” of being high risk. These statistics can be interpreted as p -values, and the BH procedure (Benjamini and Hochberg, 1995) is then applied to control the expected fraction of selected patients who will experience the event within the time horizon.

Unlike classical hypothesis testing, however, the hypotheses considered here are not statements about fixed population parameters. Instead, they are random variables depending on future event times of the patients to be screened. As a result, the statistics used as input to the BH procedure are not p -values in the classical sense. Nevertheless, this hypothesis-testing analogy is both intuitive and mathematically meaningful, and has been fruitfully adopted in recent work on selective inference in a conformal prediction setting, beginning with Jin and Candès (2023).

This approach departs from the *inductive* perspective adopted in Section 3, where the screening rule is calibrated solely using the calibration data and fixed prior to observing the cohort to be screened. Here, we instead adopt a *transductive* or cohort-adaptive perspective, in which the screening threshold parameter λ in (2) is allowed to depend not only on the calibration data but also on the covariate information of the specific cohort to which the screening rule is applied.

Concretely, we consider a cohort of m i.i.d. individuals drawn from the population of interest, independent of the fitted models \hat{S} and \hat{G} and of the calibration dataset \mathcal{D}_{cal} . We denote this (partly unobserved) cohort, or test set, by

$$\mathcal{D}_{\text{test}} := \{(X_{n+j}, T_{n+j}, C_{n+j})\}_{j=1}^m.$$

At screening time, only the covariates X_{n+1}, \dots, X_{n+m} are observed.

For each cohort patient $j \in [m]$, define the null and alternative “hypotheses”:

$$H_{n+j}^0 : T_{n+j} \leq t_0 \quad \text{vs.} \quad H_{n+j}^a : T_{n+j} > t_0, \quad (9)$$

where the null H_{n+j}^0 corresponds to patient j experiencing the event before the time horizon t_0 . Again, we emphasize that these are *random variables* rather than hypotheses about fixed population parameters. Apart from highlighting the analogy with hypothesis testing, a more precise notation would be $H_{n+j}^0 = \mathbb{I}\{T_{n+j} \leq t_0\}$.

For any cohort-specific and possibly data-dependent screening rule A , let $\hat{\mathcal{S}} \subseteq [m]$ denote the subset of cohort patients who are selected. From the hypothesis testing perspective, this can be interpreted as the set of rejected nulls. Let also $\mathcal{H}_0 := \{j \in [m] : T_{n+j} \leq t_0\}$ denote the subset of cohort patients who experience the event before the time horizon t_0 , corresponding to the set of true null hypotheses.

A key quantity of interest is the proportion of selected patients who experience the event before t_0 . To emphasize the analogy with the classical notion of *false discovery proportion* (FDP) in hypothesis testing, we refer to this quantity as the FDP, and to its expectation as the FDR.

Formally, we define the FDP and the FDR as:

$$\text{FDP} := \frac{|\widehat{\mathcal{S}} \cap \mathcal{H}_0|}{\max\{1, |\widehat{\mathcal{S}}|\}}, \quad \text{FDR} := \mathbb{E}[\text{FDP}], \quad (10)$$

where the expectation is taken with respect to both the calibration data \mathcal{D}_{cal} , on which the screening rule may depend, and the test data $\mathcal{D}_{\text{test}}$.

After describing the proposed methodology in more detail, we will show this notion of FDR provides a natural criterion for approximately solving the stochastic optimization problem in (5). In particular, FDR control encodes the desired risk constraint *in expectation*, in contrast to the high-probability guarantees pursued in Section 3.

4.2 Screening with the Benjamini–Hochberg Procedure

For each $j \in [m]$, we construct a covariate-dependent statistic $\hat{p}(X_{n+j}) \in [0, 1]$ that tends to take smaller values when the “null” event $H_{n+j}^0 : T_{n+j} \leq t_0$ does not occur. The construction of these statistics is described in Section 4.3.

Although $\hat{p}(X_{n+j})$ can be intuitively interpreted as a “ p -value” for “testing” H_{n+j}^0 , this analogy is not entirely rigorous because the hypotheses themselves are random. Following the framework of Jin and Candès (2023), we refer to these quantities as *selective conformal p -values*, both to emphasize their conformal construction and to distinguish them from more traditional conformal p -values used in other settings such as outlier detection (Bates et al., 2023).

By construction, $\hat{p}(X_{n+j})$ should satisfy the following *marginal* super-uniformity:

$$\mathbb{P}[\hat{p}(X_{n+j}) \leq \alpha, T_{n+j} \leq t_0] \leq \alpha, \quad \forall \alpha \in (0, 1). \quad (11)$$

This property ensures that smaller values of $\hat{p}(X_{n+j})$ provide evidence that $T_{n+j} \geq t_0$, and is sufficient to guarantee FDR control in the sense of (10) when the BH procedure is applied, as proved by Jin and Candès (2023).

Theorem 1 (Jin and Candès (2023)). *Define $H_{n+1}^0, \dots, H_{n+m}^0$ as in (9) and let $\hat{p}(X_{n+1}), \dots, \hat{p}(X_{n+m})$ be selective conformal p -values satisfying (11). Apply the BH procedure at level $\alpha \in (0, 1)$ to these statistics, and let $\widehat{\mathcal{S}} \subseteq [m]$ denote the resulting set of rejections. Then the FDR defined in (10) satisfies $\text{FDR} \leq \alpha$.*

Recall that applying BH to selective conformal p -values $\hat{p}(X_{n+1}), \dots, \hat{p}(X_{n+m})$ means computing an adaptive p -value threshold

$$\hat{q}(\alpha) := \max \left\{ \tau \in [0, 1] : \#\{j : \hat{p}(X_{n+j}) \leq \tau\} \geq \frac{m}{\alpha} \tau \right\}$$

and then defining the set $\widehat{\mathcal{S}}$ of selected patients as:

$$\widehat{\mathcal{S}} = \{j \in [m] : \hat{p}(X_{n+j}) \leq \hat{q}(\alpha)\}. \quad (12)$$

This FDR-calibrated screening procedure can be viewed as a special case of the general framework introduced in Section 2.2, in which the selected set for the cohort is written as $\widehat{\mathcal{S}} = \{j \in [m] : A_\lambda(X_{n+j}) = 1\}$ for screening rules of the form $A_\lambda(x) := \mathbb{I}\{\hat{z}(x) \geq \lambda\}$. Indeed, by defining the score $\hat{z}(x) := 1 - \hat{p}(x)$ and the data-adaptive threshold $\hat{\lambda} := 1 - \hat{q}(\alpha)$, the BH rule can be expressed equivalently as $\widehat{\mathcal{S}} = \{j \in [m] : \hat{z}(X_{n+j}) \geq \hat{\lambda}\}$. A key difference relative to the inductive calibration methods of Section 3 is that both components of this screening rule are data-driven:

the score \hat{z} depends on the calibration data \mathcal{D}_{cal} , as detailed in Section 4.3, while the threshold $\hat{\lambda}$ further adapts to the specific cohort through the BH procedure.

To strengthen the connection between FDR-calibrated screening and the original formulation of the calibration task as the stochastic optimization problem in (5), we now establish a direct link between FDR control via the BH procedure and control of the selected-set risk (3) in expectation. This connection makes FDR-based screening directly comparable to the high-probability calibration methods of Section 3.

Theorem 2. *Let $(\hat{p}_j, H_j^0)_{j=1}^m$ be pairs of random variables, with $\hat{p}_j \in [0, 1]$ and $H_j^0 \in \{0, 1\}$, that are i.i.d. conditional on \mathcal{D}_{cal} . For any $\tau \in [0, 1]$, define*

$$\bar{r}(\tau; \mathcal{D}_{\text{cal}}) := \mathbb{P}(H_1^0 = 1 \mid \hat{p}_1 \leq \tau, \mathcal{D}_{\text{cal}}).$$

Run BH at level α on $(\hat{p}_1, \dots, \hat{p}_m)$ and let $\hat{\mathcal{S}} \subseteq [m]$ denote the corresponding rejection set. Then the FDR, defined as in (10) with $\mathcal{H}_0 = \{j \in [m] : H_j^0 = 1\}$, satisfies

$$\text{FDR} = \mathbb{E} \left[\mathbb{P}(|\hat{\mathcal{S}}| > 0 \mid \mathcal{D}_{\text{cal}}) \cdot \bar{r} \left(\frac{\alpha |\hat{\mathcal{S}}|}{m}; \mathcal{D}_{\text{cal}} \right) \right].$$

The proof of Theorem 2 is in Supplement Section A2. To see how this result connects to the selected-set risk r in (3), note that the BH threshold $\alpha |\hat{\mathcal{S}}|/m$ corresponds to an adaptive threshold $\hat{\lambda} = 1 - \alpha |\hat{\mathcal{S}}|/m$ for the scores $\hat{z}(X_{n+j}) = 1 - \hat{p}(X_{n+j})$. Thus,

$$\bar{r} \left(\frac{\alpha |\hat{\mathcal{S}}|}{m}; \mathcal{D}_{\text{cal}} \right) = r(A_{\hat{\lambda}}; \mathcal{D}_{\text{cal}}),$$

where $A_{\hat{\lambda}}$ denotes the cohort-specific screening rule $A_{\hat{\lambda}}(X_{n+j}) := \mathbb{I}\{\hat{z}(X_{n+j}) \geq \hat{\lambda}\}$.

It follows that in regimes where $\mathbb{P}(|\hat{\mathcal{S}}| > 0 \mid \mathcal{D}_{\text{cal}})$ is close to one—corresponding to cohorts that are not too small and screening rules with non-negligible yield—FDR control is effectively equivalent to controlling the selected-set risk r in expectation.

A practical advantage of BH calibration is that it requires neither a pre-specified threshold grid nor a confidence level δ , unlike the high-probability approaches from Section 3. Instead, the user only needs to specify the target risk level α (for example, 10%). Its main limitation arises in the rare-selection regime, when $\mathbb{P}(|\hat{\mathcal{S}}| > 0)$ is small, as the FDR may then understate the conditional event rate among selected individuals. However, a simple stabilization correction can mitigate this issue: one can estimate $\mathbb{P}(|\hat{\mathcal{S}}| > 0 \mid \mathcal{D}_{\text{cal}})$ via a nonparametric bootstrap of the test-set p-values (resampling individuals from the test cohort and reapplying the BH procedure) and then abstain if the estimated probability falls below an acceptable threshold ν (e.g., $\nu = 0.9$).

Algorithm 1 summarizes this FDR-based screening procedure, including the computation of selective conformal p -values detailed in Section 4.3.

4.3 Computing Selective Conformal p -Values under Right-Censoring

To construct selective conformal p -values from right-censored data that approximately satisfy (11) under standard IPCW assumptions, we follow the approach of Sesia and Svetnik (2025b), which in turn builds on Jin and Candès (2023). We describe below a slightly enhanced version of their method, which we find often improves selection yield in practice.

For each cohort individual $j \in [m]$, we compute a *nonconformity score* Z_{n+j} intended to quantify how plausible it is that the individual survives beyond the time horizon t_0 according to the fitted survival model. Larger values of Z_{n+j} should indicate stronger evidence against $H_{n+j}^0 : T_{n+j} \leq t_0$.

Algorithm 1 FDR-conformal patient screening.

Require: Pre-trained survival model $\hat{S}(\cdot | x)$ and censoring model $\hat{G}(\cdot | x)$; right-censored calibration data $\mathcal{D}_{\text{cal}} = \{(X_i, \tilde{T}_i, E_i)\}_{i=1}^n$; test covariates $\{X_{n+1}, \dots, X_{n+m}\}$; target risk level $\alpha \in (0, 1)$; time shift parameter $\gamma \geq 0$; selection stability threshold $\nu \in [0, 1]$.

- 1: For $i \in [n]$, compute $w_i = 1/\hat{G}(\tilde{T}_i^- | X_i)$, with winsorization.
- 2: For $i \in [n]$ and $j \in [m]$, compute Z_i and Z_{n+j} as in (13), with time shift γ .
- 3: For $j \in [m]$, compute conformal p-value $\hat{p}(X_{n+j})$ as in (14).
- 4: Apply BH at level α to $\{\hat{p}(X_{n+j})\}_{j=1}^m$ and set rejection set $\hat{\mathcal{S}} \subseteq [m]$.
- 5: (*Optionally abstain*) Compute $\hat{\mathbb{P}}(|\hat{\mathcal{S}}| > 0)$ by nonparametric bootstrap over test rows; set $\hat{\mathcal{S}} = \emptyset$ if $\hat{\mathbb{P}}(|\hat{\mathcal{S}}| > 0) < \nu$.

Ensure: Selected subset of patients $\hat{\mathcal{S}} \subseteq [m]$.

A natural choice, which slightly generalizes the score defined earlier in (1), is

$$Z_{n+j} = \hat{S}(t_0 + \gamma | X_{n+j}),$$

where \hat{S} denotes the estimated survival function and $\gamma \geq 0$ is a user-specified *time shift* parameter that determines how far beyond t_0 the survival probability is evaluated. The choice $\gamma = 0$, corresponding to evaluation exactly at t_0 , is adopted in (1) and in Sesia and Svetnik (2025b); while intuitive, this choice is not always optimal. We discuss below how to tune γ to improve screening power.

To assess, in a model-agnostic manner, the statistical evidence provided by Z_{n+j} against $H_{n+j}^0 : T_{n+j} \leq t_0$, Jin and Candès (2023) propose comparing this score to analogous scores computed on the calibration data, using the observed event or censoring times instead of the fixed horizon t_0 . Specifically, we define the scores

$$Z_i = \hat{S}(\tilde{T}_i + \gamma | X_i), \quad i \in [n], \quad Z_{n+j} = \hat{S}(t_0 + \gamma | X_{n+j}), \quad j \in [m], \quad (13)$$

where $\tilde{T}_i = \min(T_i, C_i)$ denotes the observed time for calibration individual i .

Intriguingly, the calibration scores Z_1, \dots, Z_n are by construction *not* exchangeable with the cohort scores Z_{n+1}, \dots, Z_{n+m} , nor even with the subset of cohort scores corresponding to individuals with $T_{n+j} \leq t_0$. This lack of exchangeability is a defining feature of the selective conformal inference framework introduced by Jin and Candès (2023), and sharply distinguishes it from standard conformal prediction methods, which rely on full exchangeability.

The selective conformal p -value for cohort individual j is then defined as

$$\hat{p}(X_{n+j}) = \frac{1 + \sum_{i=1}^n E_i \mathbb{I}\{\tilde{T}_i \leq t_0\} w_i \mathbb{I}\{Z_i \geq Z_{n+j}\}}{1 + n}, \quad (14)$$

where each calibration observation is weighted using IPCW,

$$w_i = \frac{1}{\hat{G}(\tilde{T}_i^- | X_i)}. \quad (15)$$

Note that these selective conformal p -values depend on the event times only through \tilde{T}_i , and therefore can be evaluated in practice using right-censored calibration data.

Intuitively, $\hat{p}(X_{n+j})$ corresponds to the IPCW-adjusted empirical rank of Z_{n+j} among the calibration scores associated with individuals who experienced the event before t_0 . Smaller values of

$\hat{p}(X_{n+j})$ indicate that this cohort individual’s score is more extreme relative to such calibration cases, and hence provide stronger evidence that this individual may be low-risk.

While these selective conformal p -values may not satisfy the marginal super-uniformity property (11) exactly due to the presence of censoring, it can be shown that this property holds approximately in the large- n limit under some relatively mild regularity conditions and standard IPCW assumptions. Moreover, applying the BH procedure to these approximate selective conformal p -values yields approximate FDR control, thereby extending Theorem 1 to the right-censored setting. We refer to Sesia and Svetnik (2025b) for rigorous statements of these results.

4.4 Tuning the Time Shift Parameter γ

The time shift parameter γ appearing in the nonconformity scores (13) through the shifted survival probability $\widehat{S}(\cdot + \gamma \mid x)$ plays an important role in determining screening yield. Empirically, we find that the optimal choice of γ is often data-dependent.

To avoid introducing bias into our methodology, we recommend tuning γ using a cross-validation scheme applied to an independent dataset drawn from the same population and disjoint from the calibration data. In practice, this can be accomplished by reusing the same training data employed to fit the survival and censoring models. Details of this procedure are provided in Algorithm A5 in Supplement Section A2.

5 Numerical Experiments with Semi-Synthetic Data

We compare the proposed calibration methods using semi-synthetic data designed to mimic the structure of a real oncology study while retaining full knowledge of the underlying event times, which enables full evaluation. Specifically, we begin with real patient covariates and fit models for both the event-time and censoring-time distributions conditional on these covariates, using standard survival analysis techniques. These fitted models are then treated as generative mechanisms to simulate realistic synthetic event and censoring times.

5.1 Data Description

We examine data from the Flatiron Health Research Database (FHRD), an electronic health record-derived database comprising data from over 280 oncology practices at 800+ unique sites of care in the US, spanning the period from December 2010 to May 2023 (Ma et al., 2020; Birnbaum et al., 2020; Becker et al., 2020; Johnson et al., 2025). All data are de-identified and subject to technical and administrative safeguards to protect patient confidentiality.

We focus on a cohort of 7,000 patients diagnosed with advanced non-small cell lung cancer (aNSCLC). For each patient, 43 covariates describe demographic and socioeconomic characteristics, smoking status, vital signs, functional status, comorbidity index, tumor histology, number and location of metastatic sites, treatment history, indicators of prior laboratory assessments, and a wide range of clinical laboratory measurements. The outcome measures include a binary event indicator and the corresponding time to event or censoring.

5.2 Semi-Synthetic Data Generation

Let $X = \{X_i\}_{i=1}^{N_0}$ denote the covariate matrix from the FHRD, with $N_0 = 7,000$ rows and 43 columns. These covariates are treated as fixed design points representing the target population.

Using all available observations to approximate this population as closely as possible, we fit two separate *generative* models, respectively denoted as (\hat{S}^*, \hat{G}^*) , to estimate the conditional distribution of the survival and censoring times given the covariates. We use standard modeling approaches for this task: a Cox proportional hazards model (Cox, 1972), and a generalized random forest (GRF) survival model implemented in the `grf` R package. The censoring model \hat{G}^* is fit similar to \hat{S}^* after flipping the event indicators.

For each pair of generative models and individual i , we generate independent uniform random variables $U_i, V_i \sim \text{Uniform}(0, 1)$ and define event and censoring times:

$$T_i = \inf\{t : \hat{S}^*(t | X_i) \leq U_i\}, \quad C_i = \inf\{t : \hat{G}^*(t | X_i) \leq V_i\}.$$

Thus, conditionally independent censoring holds by construction. The observed semi-synthetic data for the i -th individual are then given by (X_i, \tilde{T}_i, E_i) , where $\tilde{T}_i = \min(T_i, C_i)$ and $E_i = \mathbb{I}\{T_i < C_i\}$. This process produces a new right-censored dataset with realistic dependence patterns and known ground-truth event times. The full resampling procedure is independently repeated $R = 100$ times.

5.3 Analysis Protocol

For each replicate of the semi-synthetic data, the observations are randomly split into a training set of size $n_{\text{tr}} = 5,000$, a calibration set of size $n_{\text{cal}} = 1,000$, and a test cohort of size $n_{\text{test}} = 1,000$. We consider four screening horizons, $t_0 \in \{2, 3, 6, 9\}$ months, and aim to select a low-risk subgroup with a target event-rate of $\alpha = 0.10$, corresponding to survival probability approximately 0.90 by time t_0 . The training data are used to fit survival and censoring models, using one of three approaches: the first two are the Cox proportional hazards model and generalized random forest also used as generative models, and the third approach is an accelerated failure time gradient boosting model implemented in the `xgboost` R package. This setup allows studying method robustness under both correctly specified and misspecified settings. In each case, the calibration data are used to calibrate the screening rule, and the data from the test cohort to evaluate performance.

We compare all methods summarized in Table 1, including three high-probability (HP) calibration methods, the FDR-based conformal approach, and two reference benchmarks, all evaluated using the same fitted survival and censoring models.

The HP methods are: *HP-Pointwise* (Section 3.2), which greedily selects the largest feasible threshold using pointwise upper confidence bounds; *HP-Uniform* (Section 3.3), which constructs simultaneous confidence bounds via Gaussian-multiplier perturbations with 1000 draws; and *HP-LTT* (Section 3.4). These methods share a common threshold grid defined by 200 quantiles of the calibration score distribution and rely on pointwise risk estimates based on asymptotic delta-method approximations, with a fallback to empirical Bernstein bounds when fewer than 10 patients are selected. Unless stated otherwise, all HP methods use a significance level of $\delta = 0.10$, and we also examine sensitivity to this choice.

The *FDR-Conformal* method (Section 4) tunes the time-shift parameter γ using the training data as described in Supplement Section A2. To align with the other calibration approaches and the interpretation of Theorem 2, this method abstains whenever a bootstrap estimate of $\mathbb{P}(|\hat{\mathcal{S}}| > 0)$ falls below 0.9.

Unless specified otherwise, all four methods use the same event-time IPCW approach, to simplify the comparison. To mitigate instability from extreme censoring, the weights are winsorized at the 99th percentile within the calibration data set.

For reference, we also report results for two benchmarks: the *model-based* baseline, which treats predicted survival probabilities as exact and selects the largest subset with average predicted survival exceeding 0.90 (using both training and calibration data for model fitting), and an *oracle*

benchmark that uses the true generative survival function $S^*(t | x)$ to select the largest subset achieving 90% average survival, representing the best attainable performance under perfect knowledge of the data-generating process.

5.4 Evaluation Metrics

For each replicate and time horizon t_0 , we record the following performance measures. The first is *yield*: the number of test patients selected by the calibrated rule. The second is the *selected-set survival rate*, defined as the proportion of selected individuals who do not experience the event by time t_0 , with the convention that if no individuals are selected then the survival rate is counted as being one. We also report the selected-set survival rate *conditionally* on having selected at least one patient. Finally, we record whether at least one selection is made in a given replicate. The empirical distribution of all these metrics is summarized across the 100 replicates.

5.5 Results

Figure 1 summarizes the results for a well-specified setting, where both the data-generating and fitted models are generalized random forests. All methods successfully achieve the target survival rate across all time horizons but differ in yield. The FDR-Conformal approach selects the most patients, typically followed by HP-Pointwise and HP-LTT, while HP-Uniform is overly conservative. At longer screening horizons, the number of selected patients naturally declines for all methods. Moreover, the conditional survival among selected patients occasionally falls slightly below the target level; this behavior reflects the limitations of asymptotic approximations, on which all these methods rely, when the effective sample size is very small. Robustness to small sample sizes could be improved by applying the finite-sample fallback more aggressively—for example, when fewer than 20–30 patients are selected instead of only below 10—at the expense of reduced yield. A detailed numerical summary of these results is reported in Table A1 in Supplement Section A3.1.

Figure 2 illustrates how the choice of significance level δ affects the behavior of HP-LTT, in the same setting as Figure 1. More conservative significance levels (e.g., $\delta = 0.05$) substantially reduce yield. In contrast, when applied with very liberal significance levels (e.g., $\delta = 0.5$), HP-LTT leads to screening rules behaving more similar to those obtained with the FDR-Conformal method. The interpretation, however, differs. The FDR-Conformal method ensures that the event rate among selected patients does not exceed 10% on average, providing an expectation-level guarantee. HP-LTT with $\delta = 0.5$, on the other hand, guarantees only that the event rate will fall below 10% in at least half of repeated experiments (i.e., with probability 0.5), offering no control over how large the event rate might be in the remaining 50% of cases. Because the event rate is bounded below by 0% but can substantially exceed the 10% target, controlling its *expected value* is more meaningful than controlling it in probability at a very low confidence level such as 50%.

Figure 3 presents results from experiments analogous to those in Figure 1, except that the survival model is now misspecified: a gradient boosting model is fitted on data generated from a random forest-based generative model. As before, the high-probability calibration methods use a significance level of $\delta = 0.1$. In this setting, the uncalibrated model selects too many patients and fails to achieve the target survival rate at longer horizons. By contrast, all calibrated methods successfully control the event rate below the 10% target, though their yields decline markedly as the time horizon t_0 increases. The relative performance ordering among valid calibration methods remains consistent with the well-specified case, with FDR-Conformal selecting the most patients on average. A detailed numerical summary is provided in Table A2 in Supplement Section A3.1. Figure A1 and Table A3 summarize qualitatively similar results obtained using the Cox model

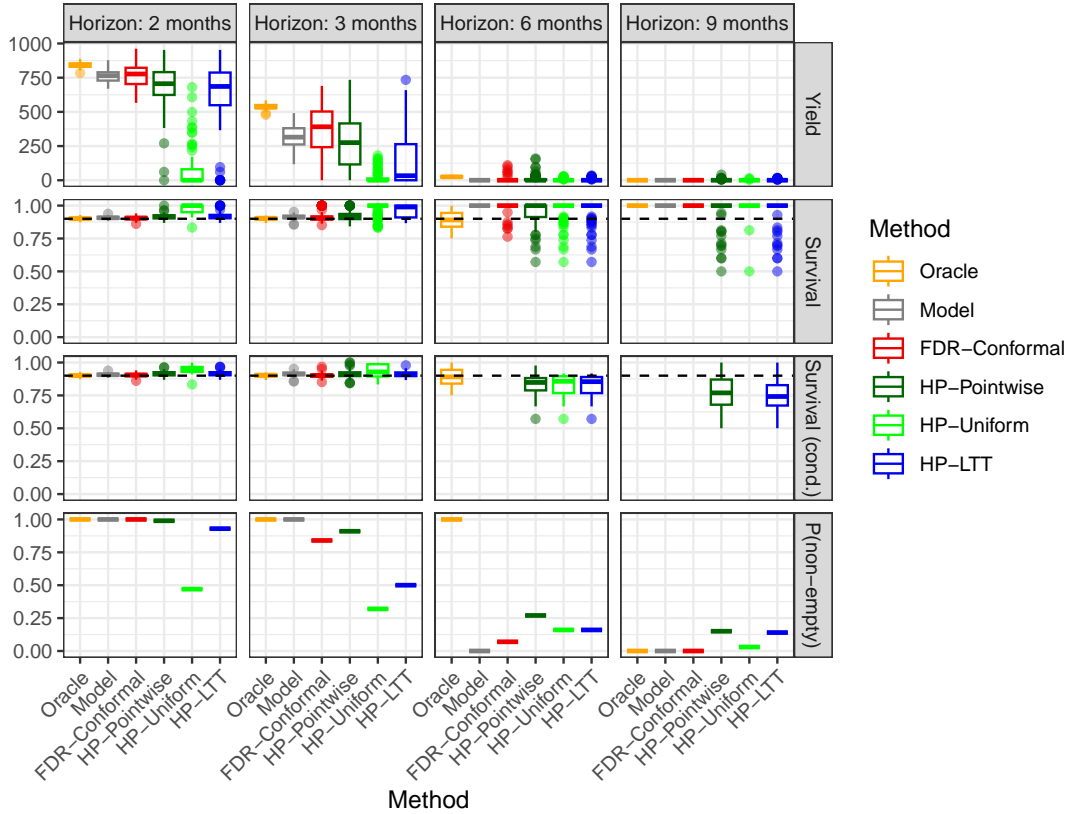


Figure 1: Summary of low-risk screening results obtained with different calibration methods on semi-synthetic data, at different screening horizons. Top row: yield. Second row: survival rate among selected patients. Third row: survival rate among selected patients, conditional on at least one patient being selected. Conditional results are not evaluated if selections occur in fewer than 10% of experiments. The dashed horizontal line denotes the target survival rate (e.g., 90%). Fourth row: proportion of experiments in which at least one patient is selected. All methods use the same survival and censoring models based on random forests. High-probability (HP) methods are applied at confidence level $\delta = 0.1$.

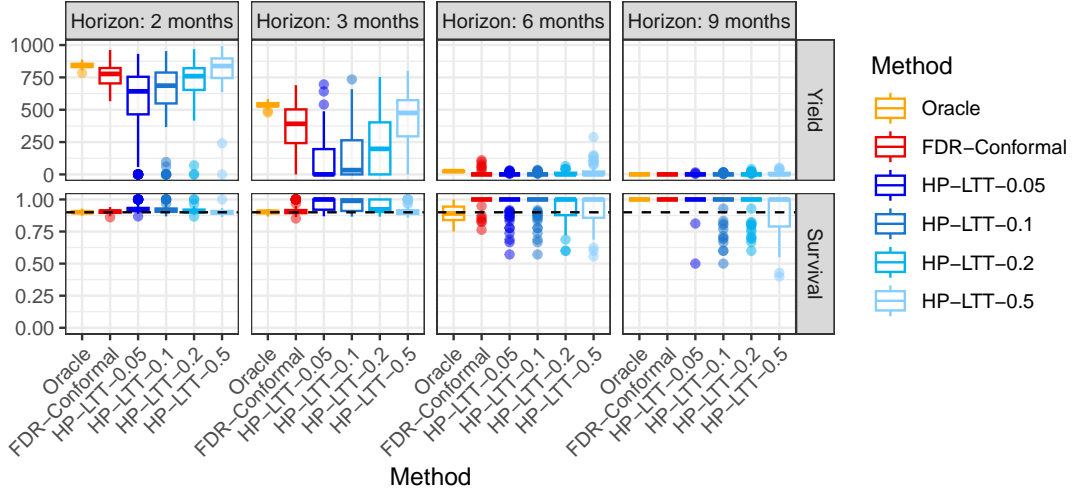


Figure 2: Summary of low-risk screening results on semi-synthetic data, as in Figure 1. Here, HP-LTT is applied at different confidence levels δ , ranging from $\delta = 0.05$ (more conservative) to $\delta = 0.5$ (more liberal).

instead of gradient boosting.

Figure 4 illustrates how the screening yield of all calibration methods tends to increase with the number of calibration samples. These results correspond to numerical experiments similar to those in Figure 1, using a fixed screening horizon of $t_0 = 2$ months and comparing all three fitted survival models considered so far: the Cox model, the generalized random forest (GRF), and gradient boosting (XGB). In this setting, FDR-Conformal performs quite similarly to the ideal oracle when the calibration sample size is large enough, while HP-LTT suffers the steepest performance decline when calibration data are scarce. Additional results following the same layout of Figure 1 but using a smaller calibration sample size ($n_{\text{cal}} = 100$) are provided in Figures A2–A3 and Table A4 in Supplement Section A3.1. These results highlight that variability increases and the number of selected patients decreases as n_{cal} becomes small. Despite this loss in precision, all procedures maintain the target survival rate on average. The uniform approach remains the most conservative calibration method, while conformal calibration consistently achieves the highest yield among valid approaches, provided that selections are not exceedingly rare.

6 Application to FHRD data

We next apply the described calibration methods directly to the FHRD data described in Section 5.1, using the true observed times and censoring indicators. We randomly divide the 7,000 observations into a training set of 5,000, a calibration set of 1,000, and a test set of 1,000, and we average all reported results over 100 independent splits. Because the event times are only partially observed, we report IPCW-adjusted point estimates of survival rates together with surrogate upper and lower bounds obtained by treating censored observations optimistically or pessimistically, respectively. Aside from this adjustment, we follow the same analysis protocol used for the semi-synthetic experiments in Section 5.3. In particular, we use a generalized random forest model to estimate the censoring distribution and evaluate three survival models (i.e., gradient boosting, the Cox model, and a generalized random forest) for estimating the event-time distribution.

Table 2 summarizes the results when gradient boosting is used to model the survival distribution,

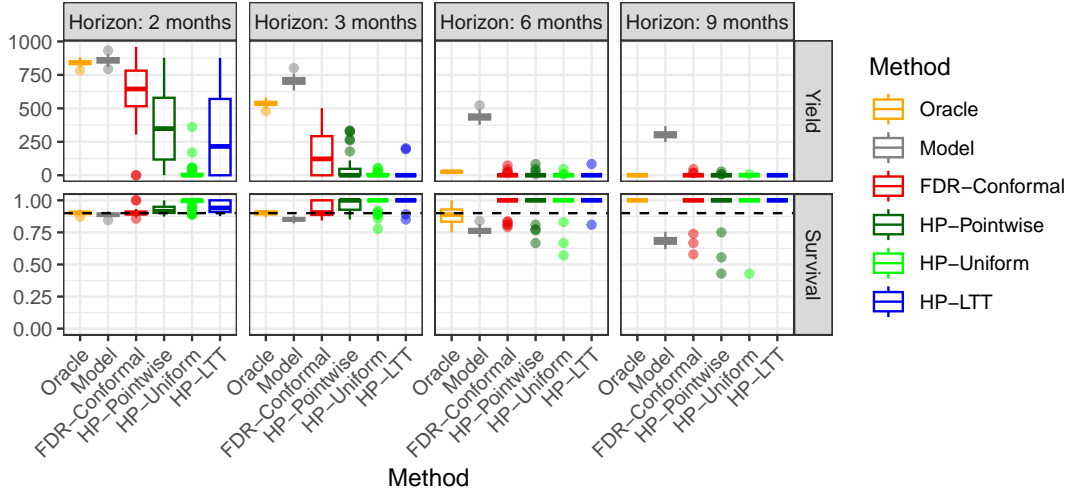


Figure 3: Summary of low-risk screening results obtained by applying different calibration methods to semi-synthetic data simulated using a random forest generative model, at different screening horizons. All methods use the same mis-specified gradient boosting survival model, which leads to lower-than-expected survival rates at long horizons if applied to select low-risk patients without calibration. Other details as in Figure 1.

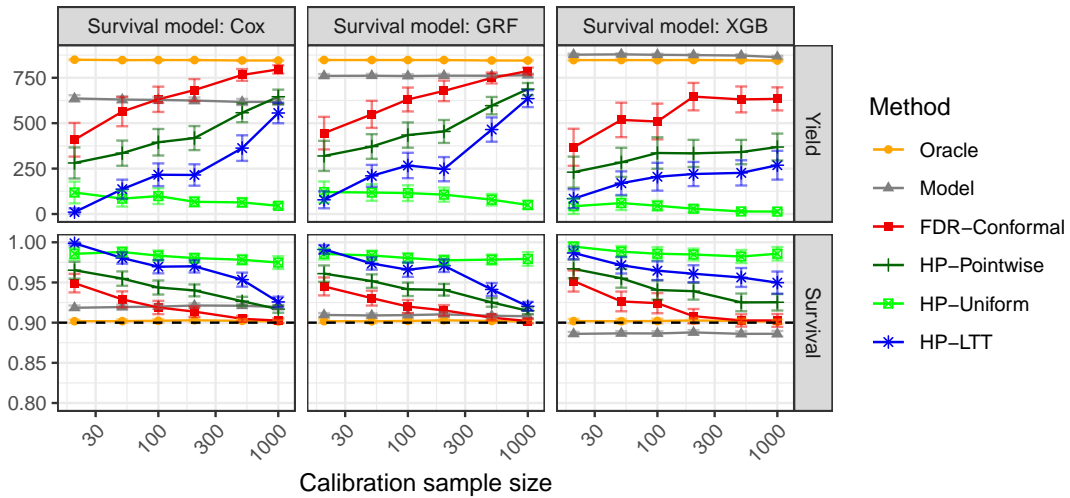


Figure 4: Average performance of low-risk screening methods on semi-synthetic data, as in Figure 1, at horizon $t_0 = 2$ months. The results are shown as a function of the calibration sample size, for different survival models. Error bars represent two standard errors.

with a visual summary provided in Figure A4 in Supplement Section A3.2. Overall, these findings closely mirror those from the semi-synthetic experiments. Across all time horizons, FDR-Conformal and all HP procedures achieve selected-set survival rates near the target level on average, including HP-Pointwise. FDR-Conformal consistently selects the most patients, typically outperforming both HP-Pointwise and HP-LTT, while HP-Uniform remains overly conservative. As the prediction horizon increases, selections become rarer and variability increases across all methods. In sharp contrast to the calibrated procedures, the uncalibrated model benchmark selects far too many patients and yields survival rates well below the desired 90% level, particularly at longer time horizons.

Table 2: Summary of low-risk screening results on FHRD data across different screening horizons. Because of censoring, survival rates cannot be evaluated exactly; instead, we report deterministic lower (LB) and upper (UB) bounds for both the marginal survival rate (Surv.) and the conditional survival rate given at least one selection (C.Surv.). We also report the fraction of trials with at least one selected patient, $P(|\hat{\mathcal{S}}| > 0)$. Each entry shows the mean and, in parentheses, two standard errors across repeated splits. Values highlighted in red indicate survival rates significantly below the 90% target, while boldface denotes the method achieving the largest number of selections among those with valid survival rates.

Method	Yield	Surv.(LB)	Surv.(UB)	C.Surv.(LB)	C.Surv.(UB)	$P(\hat{\mathcal{S}} > 0)$
Horizon: 2 months						
Model	836 (4.06)	0.88 (0.00)	0.91 (0.00)	0.88 (0.00)	0.91 (0.00)	1.00 (0.00)
FDR-Conformal	883 (15.35)	0.88 (0.00)	0.90 (0.00)	0.88 (0.00)	0.90 (0.00)	1.00 (0.00)
HP-Pointwise	790 (23.29)	0.89 (0.00)	0.92 (0.00)	0.89 (0.00)	0.92 (0.00)	1.00 (0.00)
HP-Uniform	133 (58.13)	0.96 (0.01)	0.98 (0.01)	0.94 (0.01)	0.97 (0.01)	0.63 (0.15)
HP-LTT	783 (26.91)	0.89 (0.00)	0.92 (0.00)	0.89 (0.00)	0.92 (0.00)	1.00 (0.00)
Horizon: 3 months						
Model	714 (4.73)	0.85 (0.00)	0.89 (0.00)	0.85 (0.00)	0.89 (0.00)	1.00 (0.00)
FDR-Conformal	590 (28.11)	0.86 (0.01)	0.90 (0.01)	0.86 (0.01)	0.90 (0.01)	1.00 (0.00)
HP-Pointwise	466 (32.85)	0.88 (0.01)	0.92 (0.01)	0.88 (0.01)	0.92 (0.01)	1.00 (0.00)
HP-Uniform	30 (18.38)	0.97 (0.02)	0.99 (0.01)	0.92 (0.01)	0.97 (0.01)	0.43 (0.15)
HP-LTT	375 (54.75)	0.90 (0.01)	0.93 (0.01)	0.88 (0.01)	0.92 (0.01)	0.86 (0.11)
Horizon: 6 months						
Model	505 (5.24)	0.76 (0.00)	0.83 (0.00)	0.76 (0.00)	0.83 (0.00)	1.00 (0.00)
FDR-Conformal	139 (24.65)	0.84 (0.02)	0.92 (0.01)	0.82 (0.01)	0.91 (0.01)	0.90 (0.09)
HP-Pointwise	43 (18.10)	0.92 (0.03)	0.96 (0.01)	0.84 (0.01)	0.93 (0.01)	0.49 (0.16)
HP-Uniform	4 (3.57)	0.98 (0.02)	0.99 (0.01)	0.88 (0.03)	0.96 (0.01)	0.15 (0.11)
HP-LTT	14 (13.97)	0.98 (0.02)	0.99 (0.01)	0.81 (0.01)	0.90 (0.01)	0.10 (0.09)
Horizon: 9 months						
Model	396 (5.69)	0.67 (0.01)	0.78 (0.01)	0.67 (0.01)	0.78 (0.01)	1.00 (0.00)
FDR-Conformal	17 (10.20)	0.92 (0.04)	0.96 (0.02)	0.75 (0.03)	0.88 (0.02)	0.33 (0.16)
HP-Pointwise	4 (4.25)	0.96 (0.03)	0.98 (0.02)	0.72 (0.03)	0.87 (0.02)	0.14 (0.12)
HP-Uniform	0 (0.61)	0.99 (0.01)	0.99 (0.01)	NA	NA	0.03 (0.06)
HP-LTT	0 (0.00)	1.00 (0.00)	1.00 (0.00)	NA	NA	0.00 (0.00)

Tables A5–A6 and Figures A5–A6 in Supplement Section A3.2 show analogous results for the Cox model and the generalized random forest. The trends align with those in Table 2 and Figure A4: the calibrated methods achieve survival rates near the target level on average, with FDR-Conformal typically yielding the largest selections and HP-Uniform remaining conservative. In these two settings, however, the uncalibrated model leads to a conservative rather than overly liberal screening rule. Finally, Figures A7–A9 in Supplement Section A3.2 visualize the effect of changing the significance level δ used by HP-LTT, with results analogous to those reported in Figure 2.

7 Discussion

The methods discussed in this paper extend naturally to other screening calibration problems. Firstly, they can be applied symmetrically to calibrate high-risk screening rules, by simply inverting the score inequality (Sesia and Svetnik, 2025b). Moreover, they can be adapted to handle deviations from i.i.d. sampling, such as covariate shift, via additional reweighting (Tibshirani et al., 2019; Park et al., 2024; Jin and Candès, 2025). In the future, it would be interesting to extend the FDR-Conformal method by integrating recent developments in FDR control via e-values instead of p-values (Wang and Ramdas, 2022; Vovk and Wang, 2023; Lee and Ren, 2024), a direction that could for example lead to lower algorithmic variability due to random sample splitting (Bashari et al., 2023) and the possibility of incorporating additional constraints into the patient subset selection problem (Nair et al., 2025).

Acknowledgments

The authors thank Dr. Peining Tao and Dr. Michael Johnson for preparing the analytical dataset used in this study, and Dr. Mehmet Burcu for suggesting the problem of predicting short-term survival of oncology patients.

Data Availability Statement

Software implementing the methods and experiments described in this paper is available at https://github.com/msesia/screening_calibration, along with usage examples. The data analyzed in this paper were obtained from the Flatiron Health Research Database (<https://flatiron.com/database-characterization>) and are not publicly available.

References

- Anastasios Angelopoulos, Stephen Bates, Adam Fisch, Lihua Lei, and Tal Schuster. Conformal risk control. In *International Conference on Learning Representations*, volume 2024, pages 55198–55218. ICLR, 2024a.
- Anastasios N Angelopoulos and Stephen Bates. Conformal prediction: A gentle introduction. *Foundations and trends in machine learning*, 16(4):494–591, 2023.
- Anastasios N Angelopoulos, Rina Foygel Barber, and Stephen Bates. Theoretical foundations of conformal prediction. *arXiv preprint arXiv:2411.11824*, 2024b.
- Anastasios N Angelopoulos, Stephen Bates, Emmanuel Candès, Michael I Jordan, and Lihua Lei. Learn then test: Calibrating predictive algorithms to achieve risk control. *Ann. Appl. Stat.*, 19(2):1641–1662, 2025.
- Avinash Barnwal, Hyunsu Cho, and Toby Hocking. Survival regression with accelerated failure time model in xgboost. *J. Comput. Graph. Stat.*, 31(4):1292–1302, 2022.
- Meshi Bashari, Amir Epstein, Yaniv Romano, and Matteo Sesia. Derandomized novelty detection with FDR control via conformal e-values. In *Advances in Neural Information Processing Systems*, volume 36, pages 65585–65596. NeurIPS, 2023.

- Stephen Bates, Emmanuel Candès, Lihua Lei, Yaniv Romano, and Matteo Sesia. Testing for outliers with conformal p-values. *Ann. Stat.*, 51(1):149–178, 2023.
- Peter Bauer. Multiple testing in clinical trials. *Stat. Med.*, 10(6):871–890, 1991.
- T Becker, J Weberpals, AM Jegg, WV So, A Fischer, M Weisser, F Schmich, D Rüttinger, and A Bauer-Mehren. An enhanced prognostic score for overall survival of patients with cancer derived from a large real-world cohort. *Ann. Oncol.*, 31(11):1561–1568, 2020.
- Yoav Benjamini and Yosef Hochberg. Controlling the false discovery rate: a practical and powerful approach to multiple testing. *J. R. Stat. Soc. Ser. B Methodol.*, 57(1):289–300, 1995.
- Savannah Bergquist, Gabriel A Brooks, Mary Beth Landrum, Nancy L Keating, and Sherri Rose. Uncertainty in lung cancer stage for survival estimation via set-valued classification. *Stat. Med.*, 41(19):3772–3788, 2022.
- Dimitris Bertsimas and Holly Wiberg. Machine learning in oncology: methods, applications, and challenges. *JCO Clin. Cancer Inform.*, 4:CCI–20, 2020.
- Benjamin Birnbaum, Nathan Nussbaum, Katharina Seidl-Rathkopf, Monica Agrawal, Melissa Estevez, Evan Estola, Joshua Haimson, Lucy He, Peter Larson, and Paul Richardson. Model-assisted cohort selection with bias analysis for generating large-scale cohorts from the EHR for oncology research. *arXiv preprint arXiv:2001.09765*, 2020.
- P Blanche and MP Blanche. Package ‘timeROC’: time-dependent ROC curve and AUC for censored survival data. *Vienna: R Foundation for Statistical Computing*, 2013.
- Emmanuel Candès, Lihua Lei, and Zhimei Ren. Conformalized survival analysis. *J. R. Stat. Soc. Ser. B Methodol.*, 85(1):24–45, 2023.
- Stephen R Cole and Miguel A Hernán. Constructing inverse probability weights for marginal structural models. *Am. J. Epidemiol.*, 168(6):656–664, 2008.
- David R Cox. Regression models and life-tables. *J. R. Stat. Soc. Ser. B Methodol.*, 34(2):187–202, 1972.
- Hen Davidov, Shai Feldman, Gil Shamai, Ron Kimmel, and Yaniv Romano. Conformalized survival analysis for general right-censored data. In *International Conference on Learning Representations*. ICLR, 2025.
- Rebecca Farina, Eric J Tchetgen Tchetgen, and Arun Kumar Kuchibhotla. Doubly robust and efficient calibration of prediction sets for censored time-to-event outcomes. *arXiv preprint arXiv:2501.04615*, 2025.
- Thomas R Fleming and David P Harrington. *Counting processes and survival analysis*. John Wiley & Sons, 2013.
- Yu Gui, Rohan Hore, Zhimei Ren, and Rina Foygel Barber. Conformalized survival analysis with adaptive cut-offs. *Biometrika*, 111(2):459–477, 2024.
- Patrick J Heagerty and Yingye Zheng. Survival model predictive accuracy and ROC curves. *Biometrics*, 61(1):92–105, 2005.

- Patrick J Heagerty, Thomas Lumley, and Margaret S Pepe. Time-dependent ROC curves for censored survival data and a diagnostic marker. *Biometrics*, 56(2):337–344, 2000.
- Hemant Ishwaran, Udaya B. Kogalur, Eugene H. Blackstone, and Michael S. Lauer. Random survival forests. *Ann. Appl. Stat.*, 2(3):841 – 860, 2008.
- Ying Jin and Emmanuel Candès. Selection by prediction with conformal p-values. *J. Mach. Learn. Res.*, 24(244):1–41, 2023.
- Ying Jin and Emmanuel Candès. Model-free selective inference under covariate shift via weighted conformal p-values. *Biometrika*, page asaf066, 2025.
- Michael Johnson, Peining Tao, Mehmet Burcu, John Kang, Richard Baumgartner, Junshui Ma, and Vladimir Svetnik. Creating a proxy for baseline eastern cooperative oncology group performance status in electronic health records for comparative effectiveness research in advanced non-small cell lung cancer. *JCO Clin. Cancer Inform.*, 9:e2400185, 2025.
- Jared L Katzman, Uri Shaham, Alexander Cloninger, Jonathan Bates, Tingting Jiang, and Yuval Kluger. Deepsurv: personalized treatment recommender system using a Cox proportional hazards deep neural network. *BMC Med. Res. Methodol.*, 18:1–12, 2018.
- Junu Lee and Zhimei Ren. Boosting e-BH via conditional calibration. *arXiv preprint arXiv:2404.17562*, 2024.
- Xinran Ma, Lura Long, Sharon Moon, Blythe JS Adamson, and Shrujal S Baxi. Comparison of population characteristics in real-world clinical oncology databases in the US: Flatiron Health, SEER, and NPCR. *Medrxiv*, pages 2020–03, 2020.
- Andreas Maurer and Massimiliano Pontil. Empirical bernstein bounds and sample variance penalization. *arXiv preprint arXiv:0907.3740*, 2009.
- Yash Nair, Ying Jin, James Yang, and Emmanuel Candès. Diversifying conformal selections. *arXiv preprint arXiv:2506.16229*, 2025.
- Henrik Olsson, Kimmo Kartasalo, Nita Mulliqi, Marco Capuccini, Pekka Ruusuvuori, Hemamali Samaratunga, Brett Delahunt, Cecilia Lindskog, Emiel AM Janssen, Anders Blilie, et al. Estimating diagnostic uncertainty in artificial intelligence assisted pathology using conformal prediction. *Nat. Comm.*, 13(1):7761, 2022.
- Sangdon Park, Edgar Dobriban, Insup Lee, and Osbert Bastani. PAC prediction sets under covariate shift. In *International Conference on Learning Representations*, volume 2024. ICLR, 2024.
- Yuhyun Park and LJ Wei. Estimating subject-specific survival functions under the accelerated failure time model. *Biometrika*, 90(3):717–723, 2003.
- Jing Qin, Jin Piao, Jing Ning, and Yu Shen. Conformal predictive intervals in survival analysis: a resampling approach. *Biometrics*, 81(2):ujaf063, 2025.
- James M Robins. Information recovery and bias adjustment in proportional hazards regression analysis of randomized trials using surrogate markers. *Proc. Biopharm. Sect. Am. Stat. Assoc.*, 24(3):24–33, 1993.

- James M Robins and Andrea Rotnitzky. Recovery of information and adjustment for dependent censoring using surrogate markers. In *AIDS epidemiology: methodological issues*, pages 297–331. Springer, 1992.
- Matteo Sesia and Vladimir Svetnik. Doubly robust conformalized survival analysis with right-censored data. In *International Conference on Machine Learning*. PMLR, 2025a.
- Matteo Sesia and Vladimir Svetnik. Conformal survival bands for risk screening under right-censoring. In *Proceedings of the Fourteenth Symposium on Conformal and Probabilistic Prediction with Applications*, volume 266 of *Proceedings of Machine Learning Research*, pages 464–514. PMLR, 10–12 Sep 2025b.
- John D Storey, Jonathan E Taylor, and David Siegmund. Strong control, conservative point estimation and simultaneous conservative consistency of false discovery rates: a unified approach. *J. R. Stat. Soc. Ser. B Methodol.*, 66(1):187–205, 2004.
- Ryan J Tibshirani, Rina Foygel Barber, Emmanuel Candès, and Aaditya Ramdas. Conformal prediction under covariate shift. *Advances in neural information processing systems*, 32, 2019.
- Janette Vazquez and Julio C Facelli. Conformal prediction in clinical medical sciences. *J. Healthc. Inform. Res.*, 6(3):241–252, 2022.
- David M Vock, Julian Wolfson, Sunayan Bandyopadhyay, Gediminas Adomavicius, Paul E Johnson, Gabriela Vazquez-Benitez, and Patrick J O’Connor. Adapting machine learning techniques to censored time-to-event health record data: A general-purpose approach using inverse probability of censoring weighting. *J. Biomed. Inform.*, 61:119–131, 2016.
- Vladimir Vovk and Ruodu Wang. Confidence and discoveries with e-values. *Statistical Science*, 38(2):329–354, 2023.
- Vladimir Vovk, Alexander Gammerman, and Glenn Shafer. *Algorithmic learning in a random world*, volume 29. Springer, 2005.
- Ruodu Wang and Aaditya Ramdas. False discovery rate control with e-values. *J. R. Stat. Soc. Ser. B Methodol.*, 84(3):822–852, 2022.
- Yan Yuan, Qian M Zhou, Bingying Li, Hengrui Cai, Eric J Chow, and Gregory T Armstrong. A threshold-free summary index of prediction accuracy for censored time to event data. *Stat. Med.*, 37(10):1671–1681, 2018.
- Yingye Zheng, Tianxi Cai, Margaret S Pepe, and Wayne C Levy. Time-dependent predictive values of prognostic biomarkers with failure time outcome. *J. Am. Stat. Assoc.*, 103(481):362–368, 2008.
- Yingye Zheng, Tianxi Cai, Janet L Stanford, and Ziding Feng. Semiparametric models of time-dependent predictive values of prognostic biomarkers. *Biometrics*, 66(1):50–60, 2010.

A1 Calibration via High-Probability Risk Control

A1.1 Pointwise Risk Estimation

For a fixed threshold λ , recall that the population-level *selected-set risk* is defined as

$$r(\lambda) = \frac{\theta(\lambda)}{\mu(\lambda)}, \quad \theta(\lambda) = \mathbb{E}[\mathbb{I}\{T \leq t_0\}A_\lambda(X)], \quad \mu(\lambda) = \mathbb{E}[A_\lambda(X)],$$

where $A_\lambda(X)$ indicates whether a patient with covariates X would be selected by the screening rule at threshold λ . Using the calibration data, we estimate these quantities as

$$\hat{r}(\lambda) = \frac{\hat{\theta}(\lambda)}{\hat{\mu}(\lambda)},$$

where $\hat{\theta}$ and $\hat{\mu}$ are obtained with either IPCW-ET (6) or IPCW-FT (7).

A1.1.1 Asymptotic Bounds via Delta Method

We review here how to construct an approximate $(1 - \delta)$ upper confidence bound for the true risk $r(\lambda)$ using the delta method.

Define the function $g(\theta, \mu) = \theta/\mu$, so that $\hat{r}(\lambda) = g(\hat{\theta}, \hat{\mu})$. The gradient of g is

$$\nabla g(\theta, \mu) = \begin{pmatrix} 1/\mu \\ -\theta/\mu^2 \end{pmatrix}.$$

By the multivariate delta method, the asymptotic variance of $\hat{r}(\lambda)$ is approximated by

$$\hat{\sigma}^2(\lambda) = \nabla g(\hat{v})^\top \hat{\Sigma}(\lambda) \nabla g(\hat{v}),$$

where $\hat{v} = (\hat{\theta}, \hat{\mu})^\top$ and

$$\hat{\Sigma}(\lambda) = \begin{pmatrix} \hat{\Sigma}_{\theta\theta}(\lambda) & \hat{\Sigma}_{\theta\mu}(\lambda) \\ \hat{\Sigma}_{\mu\theta}(\lambda) & \hat{\Sigma}_{\mu\mu}(\lambda) \end{pmatrix}$$

denotes the empirical covariance matrix of $(\hat{\theta}(\lambda), \hat{\mu}(\lambda))$. Each block in $\hat{\Sigma}(\lambda)$ is estimated from individual sample contributions:

$$\hat{\Sigma}_{ab}(\lambda) = \frac{1}{n} \sum_{i=1}^n (\psi_i^{(a)}(\lambda) - \bar{\psi}^{(a)}(\lambda))(\psi_i^{(b)}(\lambda) - \bar{\psi}^{(b)}(\lambda)), \quad a, b \in \{\theta, \mu\}.$$

The terms $\psi_i^{(\theta)}$ and $\psi_i^{(\mu)}$ represent each subject's contribution to the estimators of θ and μ , centered by their sample means. When using event-time weighting, these take the form:

$$\psi_i^{(\theta)} = A_\lambda(X_i) \frac{\mathbb{I}(\tilde{T}_i \leq t_0, E_i = 1)}{\hat{G}(\tilde{T}_i^- | X_i)} - \hat{\theta}_{\text{et}}(\lambda), \quad \psi_i^{(\mu)} = A_\lambda(X_i) - \hat{\mu}(\lambda).$$

Alternatively, under fixed-time weighting:

$$\psi_i^{(\theta)} = A_\lambda(X_i) \left(1 - \frac{\mathbb{I}(\tilde{T}_i \geq t_0)}{\hat{G}(t_0 | X_i)} \right) - \hat{\theta}_{\text{ft}}(\lambda), \quad \psi_i^{(\mu)} = A_\lambda(X_i) - \hat{\mu}(\lambda).$$

Expanding the expression for the asymptotic variance of $\hat{r}(\lambda)$ gives:

$$\hat{\sigma}^2(\lambda) = \frac{\hat{\Sigma}_{\theta\theta}(\lambda)}{\hat{\mu}^2(\lambda)} - 2 \frac{\hat{\theta}(\lambda)}{\hat{\mu}^3(\lambda)} \hat{\Sigma}_{\theta\mu}(\lambda) + \frac{\hat{\theta}^2(\lambda)}{\hat{\mu}^4(\lambda)} \hat{\Sigma}_{\mu\mu}(\lambda).$$

Equivalently, this can be written as a single sample variance:

$$\hat{\sigma}^2(\lambda) = \frac{1}{n} \sum_{i=1}^n \left(\frac{\psi_i^{(\theta)}(\lambda)}{\hat{\mu}(\lambda)} - \frac{\hat{\theta}(\lambda)}{\hat{\mu}^2(\lambda)} \psi_i^{(\mu)}(\lambda) \right)^2.$$

Finally, the $(1 - \delta)$ one-sided upper confidence bound for the selected-set risk is

$$\text{UCB}^{\text{pt}}(\lambda; \delta) = \hat{r}(\lambda) + z_{1-\delta} \frac{\hat{\sigma}(\lambda)}{\sqrt{n}},$$

where $z_{1-\delta}$ is the $(1 - \delta)$ quantile of the standard normal distribution.

In practice, we apply this method with mild winsorization of the weights, capping the top 1% at the 99th percentile. When $\hat{\mu}(\lambda)$ is extremely small (e.g., $< 10/n$), we revert to the more conservative finite-sample upper bound described in Appendix A1.1.3.

A1.1.2 Asymptotic Bounds via Nonparametric Bootstrap

As an alternative to the delta method, one may construct a nonparametric bootstrap upper confidence bound for $r(\lambda)$ by resampling the calibration data as outlined by Algorithm A1. Like the delta-method approximation, the bootstrap relies on large-sample asymptotics; therefore, if $\hat{\mu}(\lambda)$ is very small (e.g., $< 10/n$), we recommend reverting to the more conservative finite-sample upper bound described in Appendix A1.1.3.

Algorithm A1 Nonparametric bootstrap pointwise upper confidence bound.

Require: Pre-trained screening rule $A_\lambda : \mathcal{X} \mapsto \{0, 1\}$, calibration data $\mathcal{D}_{\text{cal}} = \{(X_i, \tilde{T}_i, E_i)\}_{i=1}^n$; fitted censoring model $\hat{G}(\cdot | X)$; number of bootstrap replicates B ; confidence level δ ; IPCW flavor **et** or **ft**.

- 1: **for** $b = 1, \dots, B$ **do**
- 2: Resample n calibration triples $\{(X_i^{*(b)}, \tilde{T}_i^{*(b)}, E_i^{*(b)})\}_{i=1}^n$ with replacement from \mathcal{D}_{cal} .
- 3: Recompute $\hat{\theta}^{*(b)}(\lambda)$ and $\hat{\mu}^{*(b)}(\lambda)$ using the same IPCW weights as in (6) or (7).
- 4: Form the bootstrap replicate $\hat{r}^{*(b)}(\lambda) = \hat{\theta}^{*(b)}(\lambda) / \hat{\mu}^{*(b)}(\lambda)$.
- 5: **end for**
- 6: Compute

$$\text{UCB}^{\text{boot}}(\lambda; \delta) = \text{Quantile}_{1-\delta}(\{\hat{r}^{*(b)}(\lambda)\}_{b=1}^B). \quad (\text{A16})$$

- 7: If $n_{\text{sel}}(\lambda) = \sum_i A_i(\lambda)$ is small (e.g., < 10), replace $\text{UCB}^{\text{boot}}(\lambda; \delta)$ with a conservative finite-sample bound.

Ensure: $(1 - \delta)$ pointwise upper confidence bound $\text{UCB}^{\text{boot}}(\lambda; \delta)$ for $r(\lambda)$.

A1.1.3 Finite-Sample Bounds via Empirical Bernstein Inequality

When the number of selected samples is very small, asymptotic approximations such as the delta-method or bootstrap can no longer be justified. In such cases, we can construct a finite-sample

upper confidence bound for $r(\lambda) = \theta(\lambda)/\mu(\lambda)$ by combining an empirical-Bernstein concentration inequality for the numerator $\theta(\lambda)$ with an exact Clopper-Pearson lower bound for the selection fraction $\mu(\lambda)$.

For concreteness, we describe the event-time IPCW case; the fixed-time case is similar. Let $Z_i(\lambda) = A_\lambda(X_i) w_i^{\text{et}}$ and $w_i^{\text{et}} = 1/\widehat{G}(\widetilde{T}_i^- | X_i)$, so that $\hat{\theta}(\lambda)$ can be written as $\hat{\theta}(\lambda) = \frac{1}{n} \sum_{i=1}^n Z_i$. Assume the weights are truncated at an upper bound M to stabilize the estimator; i.e., $w_i^{\text{et}} \leq M$ almost-surely. In practice, the constant M can be estimated empirically using the maximum of the weights in the calibration sample, after winsorization. The sample variance of the weighted contributions is given by

$$\hat{v}(\lambda) = \frac{1}{n-1} \sum_{i=1}^n (Z_i(\lambda) - \hat{\theta}(\lambda))^2.$$

The empirical-Bernstein inequality of Maurer and Pontil (2009) then implies that, with probability at least $1 - \delta/2$,

$$\theta(\lambda) \leq \hat{\theta}(\lambda) + \sqrt{\frac{2\hat{v}(\lambda) \log(4/\delta)}{n}} + \frac{7M \log(4/\delta)}{3(n-1)}. \quad (\text{A17})$$

For the denominator, note that $n\hat{\mu}(\lambda) = \sum_{i=1}^n A_\lambda(X_i)$ follows a Binomial($n, \mu(\lambda)$) distribution. An exact $(1 - \delta/2)$ lower confidence bound for $\mu(\lambda)$ is therefore

$$\hat{\mu}_{\text{low}}(\lambda; \delta) = \Psi_{\text{low}}(n, n\hat{\mu}(\lambda), \delta), \quad (\text{A18})$$

where $\Psi_{\text{low}}(n, k, \delta)$ is defined implicitly by

$$\text{pbinom}(k-1; n, \Psi_{\text{low}}(n, k, \delta)) = 1 - \delta,$$

and **pbinom** denotes the cumulative distribution function of the binomial distribution.

Combining the numerator bound (A17) and the denominator bound (A18) yields a finite-sample $(1 - \delta)$ one-sided upper confidence bound for the selected-set risk:

$$\text{UCB}^{\text{fs}}(\lambda; \delta) = \frac{\hat{\theta}_{\text{upp}}(\lambda; \delta/2)}{\hat{\mu}_{\text{low}}(\lambda; \delta/2)}, \quad (\text{A19})$$

where $\hat{\theta}_{\text{upp}}(\lambda; \delta/2)$ denotes the empirical-Bernstein upper bound in (A17). In practice, we recommend applying UCB^{fs} whenever $n_{\text{sel}}(\lambda) = \sum_i A_\lambda(X_i) < 10$.

A1.2 Greedy Pointwise Calibration

Algorithm A2 Greedy pointwise calibration

Require: Pre-trained screening rule $A_\lambda : \mathcal{X} \mapsto \{0, 1\}$ with parameter λ , calibration data $\mathcal{D}_{\text{cal}} = \{(X_i, \tilde{T}_i, E_i)\}_{i=1}^n$; censoring model $\hat{G}(\cdot | x)$; target risk level $\alpha \in (0, 1)$; confidence level $\delta \in (0, 1)$; grid $\Lambda = \{\lambda_1, \dots, \lambda_K\} \subset [0, 1]$; IPCW flavor **et** or **ft**; winsorization level τ (e.g., 1%).

- 1: Compute $\hat{\theta}(\lambda)$, $\hat{\mu}(\lambda)$ and $\hat{r}(\lambda) = \hat{\theta}(\lambda)/\hat{\mu}(\lambda)$ using winsorized IPCW as in (6) or (7).
- 2: Compute $\text{UCB}^{\text{pt}}(\lambda; \delta)$ (e.g., delta-method or finite-sample if $n_{\text{sel}}(\lambda) = \sum_i A_i(\lambda) \leq 10$).
- 3: Define the feasible set $\mathcal{F} \leftarrow \{\lambda \in \Lambda : \text{UCB}^{\text{pt}}(\lambda; \delta) \leq \alpha\}$.
- 4: If $\mathcal{F} = \emptyset$, set $\hat{\lambda} \leftarrow \text{NA}$. Otherwise choose $\hat{\lambda} \leftarrow \arg \max_{\lambda \in \mathcal{F}} n_{\text{sel}}(\lambda)$.

Ensure: Calibrated screening rule $A_{\hat{\lambda}}$.

A1.3 Conservative Uniform Calibration

The simplest way to obtain a UCB for $r(\lambda)$ that holds simultaneously with high probability across all $\lambda \in \Lambda$ is to apply the pointwise estimation methods from Section 3.1 with a Bonferroni correction. Specifically, the pointwise confidence level δ is replaced by the more conservative value δ/K , where $K = |\Lambda|$. The calibrated threshold is then chosen as

$$\hat{\lambda}_{\text{Bonferroni}} \in \arg \max_{\lambda \in \Lambda} \{ \hat{\mu}(\lambda) : \text{UCB}^{\text{pt}}(\lambda; \delta/|\Lambda|) \leq \alpha \},$$

where $\text{UCB}^{\text{pt}}(\lambda; \delta)$ represents a level- δ pointwise upper confidence bound for $r(\lambda)$, computed with any of the methods from Section 3.1. This Bonferroni correction guarantees $\mathbb{P}[r(\hat{\lambda}_{\text{Bonferroni}}) > \alpha] \leq \delta$, but tends to be overly conservative in practice, resulting in inefficient screening rules that tend to select fewer truly low-risk patients than would be feasible under less restrictive calibration. The source of this problem is that the Bonferroni correction does not account for the often strong dependencies between the estimation problems corresponding to different candidate thresholds $\lambda \in \Lambda$.

A less conservative alternative is the Gaussian multiplier (perturbation) approach, which constructs a joint confidence band by simulating correlated random fluctuations of the estimated risk across all $\lambda \in \Lambda = \{\lambda_1, \dots, \lambda_K\}$. This method builds on the same influence-function linearization that underlies the delta-method variance estimator (see Appendix A1.1 for additional details): for each individual i , we compute an estimated contribution $\phi_i(\lambda_k)$ that approximates the influence of observation i on $\hat{r}(\lambda_k)$, for all $k \in [K]$.

To approximate the joint sampling variability of $\hat{r}(\lambda_k)_{k=1}^K$, we repeatedly simulate random perturbations of these influence-function contributions. Let $\xi_i^{(b)} \sim \mathcal{N}(0, 1)$ denote independent standard normal random variables, sampled independently across bootstrap iterations $b = 1, \dots, B$ and individuals $i = 1, \dots, n$. For each iteration, we form the perturbed statistics

$$Z_k^{(b)} = \frac{1}{\sqrt{n}} \sum_{i=1}^n \xi_i^{(b)} \phi_i(\lambda_k), \quad \xi_i^{(b)} \stackrel{\text{i.i.d.}}{\sim} \mathcal{N}(0, 1),$$

and record the maximum fluctuation across thresholds, $T^{(b)} = \max_{k \leq K} |Z_k^{(b)}|$. The $(1 - \delta)$ quantile $q_{1-\delta}$ of $T^{(b)}_{b=1}^B$ provides a joint correction factor for the entire grid. This defines a uniform half-width

$$h_{\text{GM}} = q_{1-\delta}/\sqrt{n}, \quad \text{UCB}^{\text{GM}}(\lambda_k; \delta) = \hat{r}(\lambda_k) + h_{\text{GM}}, \quad k = 1, \dots, K,$$

The calibrated threshold is then chosen as

$$\hat{\lambda}_{\text{GM}} \in \arg \max_{\lambda \in \Lambda} \{ \hat{\mu}(\lambda) : \text{UCB}^{\text{GM}}(\lambda; \delta) \leq \alpha \}.$$

Because all thresholds share the same simulated perturbations, this approach automatically captures the correlation between neighboring $\hat{r}(\lambda)$ values. As a result, the uniform confidence bounds are often substantially tighter than the Bonferroni bounds when $\hat{r}(\lambda)$ varies smoothly with λ , leading to more powerful screening rules.

Algorithm A3 Conservative uniform calibration

Require: Pre-trained screening rule $A_\lambda : \mathcal{X} \mapsto \{0, 1\}$ with parameter λ , calibration data $\mathcal{D}_{\text{cal}} = \{(X_i, \tilde{T}_i, E_i)\}_{i=1}^n$; censoring model $\hat{G}(\cdot | x)$; target risk level α ; confidence level δ ; grid $\Lambda = \{\lambda_1, \dots, \lambda_K\}$; IPCW flavor **et** or **ft**; band type **band** $\in \{\text{bonferroni}, \text{multiplier}\}$; number of draws B ; winsorization level τ .

- 1: Compute $\hat{\theta}(\lambda_k)$, $\hat{\mu}(\lambda_k)$, and $\hat{r}(\lambda_k) = \hat{\theta}(\lambda_k)/\hat{\mu}(\lambda_k)$ for all $\lambda_k \in \Lambda$ using winsorized IPCW as in (6) or (7).
- 2: Construct uniform upper confidence bounds on Λ :
 - **bonferroni**: $\text{UCB}^{\text{uni}}(\lambda_k) \leftarrow \text{UCB}^{\text{pt}}(\lambda_k; \delta/K)$.
 - **multiplier**: draw $\xi_i^{(b)} \sim \mathcal{N}(0, 1)$, compute $Z_k^{(b)} = n^{-1/2} \sum_i \xi_i^{(b)} \phi_i(\lambda_k)$, set $q_{1-\delta}$ to the $(1 - \delta)$ quantile of $T^{(b)} = \max_k |Z_k^{(b)}|$, and $\text{UCB}^{\text{uni}}(\lambda_k) = \hat{r}(\lambda_k) + q_{1-\delta}/\sqrt{n}$.
- 3: Define the feasible set $\mathcal{F} \leftarrow \{\lambda_k \in \Lambda : \text{UCB}^{\text{uni}}(\lambda_k; \delta) \leq \alpha\}$.
- 4: If $\mathcal{F} = \emptyset$, set $\hat{\lambda} \leftarrow \text{NA}$; otherwise $\hat{\lambda} \leftarrow \arg \max_{\lambda \in \mathcal{F}} n_{\text{sel}}(\lambda)$, where $n_{\text{sel}}(\lambda) = \sum_i A_i(\lambda)$.

Ensure: Calibrated screening rule $A_{\hat{\lambda}}$.

A1.4 Learn-then-Test (LTT) Calibration

Algorithm A4 Learn-Then-Test (LTT) calibration

Require: Pre-trained screening rule $A_\lambda : \mathcal{X} \mapsto \{0, 1\}$; calibration data $\mathcal{D}_{\text{cal}} = \{(X_i, \tilde{T}_i, E_i)\}_{i=1}^n$; survival model $\hat{S}(\cdot | x)$; censoring model $\hat{G}(\cdot | x)$; target risk level α ; confidence level δ ; IPCW flavor **et** or **ft**; winsorization level τ .

- 1: Compute calibration scores $Z_i = \hat{S}(t_0 | X_i)$, and IPCW weights winsorized at level τ .
- 2: Define two anchor thresholds $\lambda_0^{(1)} = 1 - \alpha$ and $\lambda_0^{(2)} = 1 - \alpha/2$. For each anchor $l \in \{1, 2\}$, construct a decreasing sequence $\Lambda^{(l)} = \{\lambda_0^{(l)} > \lambda_1^{(l)} > \dots > \lambda_K^{(l)}\}$ by setting $\lambda_j^{(l)}$ to successive lower quantiles of $\{Z_i\}$ below $\lambda_0^{(l)}$ (e.g., 95th, 92nd, 90th, \dots percentiles).
- 3: Set per-path confidence level $\delta_\star = \delta/2$.
- 4: **for** $l = 1, 2$ **do**
- 5: Initialize $\hat{\lambda}_{\text{LTT}}^{(l)} \leftarrow 1$.
- 6: **for** $\lambda \in \Lambda^{(l)}$ (in decreasing order) **do**
- 7: Compute pointwise upper confidence bound $\text{UCB}^{\text{pt}}(\lambda; \delta_\star)$ for $r(\lambda)$.
- 8: **if** $\text{UCB}^{\text{pt}}(\lambda; \delta_\star) \leq \alpha$ **then**
- 9: Set $\hat{\lambda}_{\text{LTT}}^{(l)} \leftarrow \lambda$.
- 10: **else**
- 11: **break**
- 12: **end if**
- 13: **end for**
- 14: **end for**
- 15: Set $\hat{\lambda}_{\text{LTT}} = \min\{\hat{\lambda}_{\text{LTT}}^{(1)}, \hat{\lambda}_{\text{LTT}}^{(2)}\}$.

Ensure: Calibrated screening rule $A_{\hat{\lambda}_{\text{LTT}}}$.

A2 Calibration via FDR Control and Conformal Inference

Proof of Theorem 2. To simplify the notation, let $A_j := \mathbb{I}[j \in \widehat{\mathcal{S}}]$ and $R := \sum_{j=1}^m A_j = |\widehat{\mathcal{S}}|$.

By construction, the BH cutoff equals $\alpha k/m$ on the event $\{R = k\}$, for any $k \in [m]$; hence,

$$A_j = \mathbb{I}[\hat{p}_j \leq \alpha k/m] \quad \text{on } \{R = k\}. \quad (\text{A20})$$

For each j , let $\tilde{R}^{(j)}$ denote the BH rejection count after replacing \hat{p}_j by 0. It is a known and easily verified fact that, for every j and $k \in [m]$,

$$A_j \mathbb{I}[R = k] = A_j \mathbb{I}[\tilde{R}^{(j)} = k] \quad \text{a.s.} \quad (\text{A21})$$

By the definition of FDR given in (10),

$$\begin{aligned} \text{FDR} &= \mathbb{E} \left[\frac{\sum_{j=1}^m N_j A_j}{\max(R, 1)} \right] \\ &= \sum_{j=1}^m \sum_{k=1}^m \frac{1}{k} \mathbb{E} [N_j A_j \mathbb{I}[R = k]] \\ &= \sum_{j=1}^m \sum_{k=1}^m \frac{1}{k} \mathbb{E} [N_j A_j \mathbb{I}[\tilde{R}^{(j)} = k]]. \end{aligned}$$

Using (A20) together with (A21),

$$A_j \mathbb{I}[\tilde{R}^{(j)} = k] = \mathbb{I}[\hat{p}_j \leq \alpha k/m] \mathbb{I}[\tilde{R}^{(j)} = k] \quad \text{a.s.}$$

Hence

$$\text{FDR} = \sum_{j=1}^m \sum_{k=1}^m \frac{1}{k} \mathbb{E} [N_j \mathbb{I}[\hat{p}_j \leq \alpha k/m] \mathbb{I}[\tilde{R}^{(j)} = k]].$$

Let

$$\mathcal{F}_{j,k} := \sigma(\mathcal{D}_{\text{cal}}, \{\hat{p}_\ell : \ell \neq j\}, \mathbb{I}[\hat{p}_j \leq \alpha k/m]).$$

Since $\tilde{R}^{(j)}$ depends only on \mathcal{D}_{cal} and $\{\hat{p}_\ell : \ell \neq j\}$, the indicator $\mathbb{I}[\tilde{R}^{(j)} = k]$ is $\mathcal{F}_{j,k}$ -measurable.

Applying the tower property,

$$\begin{aligned} \text{FDR} &= \sum_{j=1}^m \sum_{k=1}^m \frac{1}{k} \mathbb{E} \left[\mathbb{E} [N_j \mathbb{I}[\hat{p}_j \leq \alpha k/m] \mid \mathcal{F}_{j,k}] \mathbb{I}[\tilde{R}^{(j)} = k] \right] \\ &= \sum_{j=1}^m \sum_{k=1}^m \frac{1}{k} \mathbb{E} \left[\mathbb{I}[\hat{p}_j \leq \alpha k/m] \mathbb{E} [N_j \mid \mathcal{F}_{j,k}, \hat{p}_j \leq \alpha k/m] \mathbb{I}[\tilde{R}^{(j)} = k] \right]. \end{aligned}$$

By conditional independence of (\hat{p}_j, N_j) from $\{\hat{p}_\ell : \ell \neq j\}$ given \mathcal{D}_{cal} ,

$$\mathbb{E} [N_j \mid \mathcal{F}_{j,k}, \hat{p}_j \leq \alpha k/m] = \mathbb{P} [N_j = 1 \mid \mathcal{D}_{\text{cal}}, \hat{p}_j \leq \alpha k/m].$$

By the assumption that the pairs $(\hat{p}_j, N_j)_{j=1}^m$ are i.i.d. conditional on \mathcal{D}_{cal} , this equals $\bar{r}(\alpha k/m; \mathcal{D}_{\text{cal}})$. Substituting,

$$\text{FDR} = \sum_{j=1}^m \sum_{k=1}^m \frac{1}{k} \mathbb{E} \left[\mathbb{I}[\hat{p}_j \leq \alpha k/m] \bar{r}(\alpha k/m; \mathcal{D}_{\text{cal}}) \mathbb{I}[\tilde{R}^{(j)} = k] \right].$$

Using again (A20) and (A21) to replace $\mathbb{I}[\hat{p}_j \leq \alpha k/m] \mathbb{I}[\tilde{R}^{(j)} = k]$ with $A_j \mathbb{I}[R = k]$, we get

$$\text{FDR} = \sum_{j=1}^m \sum_{k=1}^m \frac{1}{k} \mathbb{E} [A_j \bar{r}(\alpha k/m; \mathcal{D}_{\text{cal}}) \mathbb{I}[R = k]].$$

Finally, on $\{R = k\}$ we have $\sum_{j=1}^m A_j = k$, and therefore

$$\text{FDR} = \sum_{k=1}^m \mathbb{E} [\bar{r}(\alpha k/m; \mathcal{D}_{\text{cal}}) \mathbb{I}[R = k]] = \mathbb{E} \left[\bar{r} \left(\frac{\alpha R}{m}; \mathcal{D}_{\text{cal}} \right) \mathbb{I}[R > 0] \right].$$

The result is then obtained by applying once again the tower property conditional on D_{cal} . \square

Algorithm A5 Cross-validation to tune the time shift parameter γ for Algorithm 1

Require: Tuning dataset $\mathcal{D}_{\text{tune}} = \{(X_i, \tilde{T}_i, E_i)\}_{i=1}^N$ (independent of final calibration data); pre-fitted survival model $\hat{S}(\cdot | x)$ and censoring model $\hat{G}(\cdot | x)$; horizon t_0 ; target level α ; candidate grid Γ ; number of repetitions R ; split fractions $(\pi_{\text{cal}}, \pi_{\text{test}})$; evaluation criterion $\in \{\text{BH}, \text{Fisher}\}$.

- 1: **for** $r = 1$ to R **do**
- 2: Randomly split $\mathcal{D}_{\text{tune}}$ into disjoint subsets $D_{\text{tune}}^{\text{train}}$, $D_{\text{tune}}^{\text{cal}}$, and $D_{\text{tune}}^{\text{test}}$ according to fractions $(1 - \pi_{\text{cal}} - \pi_{\text{test}}, \pi_{\text{cal}}, \pi_{\text{test}})$.
- 3: Optionally refit smaller models \hat{S}_r, \hat{G}_r on $D_{\text{tune}}^{\text{train}}$ (otherwise use \hat{S}, \hat{G}).
- 4: **for** each $\gamma \in \Gamma$ **do**
- 5: Apply Algorithm 1 using calibration set $D_{\text{tune}}^{\text{cal}}$, test set $D_{\text{tune}}^{\text{test}}$, and time shift γ , obtaining conformal p -values $\{\hat{p}_j\}$.
- 6: Compute the performance score $J_r(\gamma)$: number of BH rejections at level α , or Fisher statistic $J_r(\gamma) = -2 \sum_j \log \hat{p}_j$.
- 7: **end for**
- 8: **end for**
- 9: Aggregate scores $\bar{J}(\gamma) = R^{-1} \sum_{r=1}^R J_r(\gamma)$.
- 10: Select $\gamma^* = \arg \max_{\gamma \in \Gamma} \bar{J}(\gamma)$ (break ties by smallest γ).

Ensure: Tuned time shift γ^* .

A2.1 Additional Implementation Details

The time shift parameter γ used by Algorithm 1 to compute $Z_i = \hat{S}(\tilde{T}_i + \gamma | X_i)$ and $Z_{n+j} = \hat{S}(t_0 + \gamma | X_{n+j})$ should be tuned on a tuning data set *independent* of the calibration data in order to maximize power without invalidating any guarantees.

In practice, we tune γ as described below and summarized by Algorithm A5. First, define a grid Γ of candidate values (e.g., $\{0\}$ together with several quantiles of the observed event times). Then, repeatedly split the training data (assumed independent of the calibration data) into three subsets: a tuning-training set for model fitting, a tuning-calibration set for conformal calibration, and a tuning-test set for evaluation. On each split, fit smaller survival and censoring models using the tuning-training subset, then apply Algorithm 1 for each candidate value of γ using the tuning-calibration and tuning-test subsets in place of the true calibration and test sets. Measure performance on the tuning-test set either by (i) the yield at level α , or (ii) in lower-power settings, by the smoother Fisher combination statistic $-2 \sum_i \log \hat{p}_i$, where \hat{p}_i denote the conformal p -values for the tuning-test set. In our experiments, we adopt the Fisher criterion by default and set the stability threshold for the optional abstention rule to $\nu = 0.9$ when estimating $\mathbb{P}(|\hat{\mathcal{S}}| > 0)$ via bootstrap. Then, we average the performance score across several random splits, and select

$$\gamma^* = \arg \max_{\gamma \in \Gamma} \text{AverageScore}(\gamma).$$

Finally, fix $\gamma = \gamma^*$ and run Algorithm 1 on the actual calibration and test sets. For computational efficiency, we can precompute $\hat{S}(\cdot | X)$ on a fine time grid and use interpolation to evaluate $\hat{S}(\tilde{T}_i + \gamma | X_i)$ and $\hat{S}(t_0 + \gamma | X_i)$ for all $\gamma \in \Gamma$, avoiding repeated model calls.

A3 Additional Numerical Results

A3.1 Experiments with Simulated Data

Table A1: Detailed numerical summary of results corresponding to Figure 1. Each entry shows the mean and (in parenthesis) two standard errors across repeated trials. Values in bold indicate the method selecting the most patients at each time (among those with valid survival rate). Conditional results are not evaluated if selections occur in fewer than 10% of experiments.

Method	Yield	Survival	Survival (cond.)	$P(\hat{S} > 0)$
Horizon: 2 months				
Oracle	841 (3.69)	1 (0.00)	1 (0.00)	1 (0.00)
Model	760 (8.35)	0.91 (0.00)	0.91 (0.00)	1.00 (0.00)
FDR-Conformal	770 (18.01)	0.90 (0.00)	0.90 (0.00)	1.00 (0.00)
HP-Pointwise	685 (30.88)	0.91 (0.00)	0.91 (0.00)	0.99 (0.02)
HP-Uniform	71 (27.39)	0.98 (0.01)	0.95 (0.01)	0.47 (0.10)
HP-LTT	629 (46.07)	0.92 (0.01)	0.91 (0.00)	0.93 (0.05)
Horizon: 3 months				
Oracle	538 (4.16)	1 (0.00)	1 (0.00)	1 (0.00)
Model	324 (14.95)	0.91 (0.00)	0.91 (0.00)	1.00 (0.00)
FDR-Conformal	355 (39.78)	0.92 (0.01)	0.90 (0.00)	0.84 (0.07)
HP-Pointwise	277 (37.31)	0.92 (0.01)	0.91 (0.01)	0.91 (0.06)
HP-Uniform	19 (8.15)	0.98 (0.01)	0.93 (0.01)	0.32 (0.09)
HP-LTT	150 (37.34)	0.96 (0.01)	0.91 (0.00)	0.50 (0.10)
Horizon: 6 months				
Oracle	25 (1.17)	1 (0.01)	1 (0.01)	1 (0.00)
Model	0 (0.00)	1.00 (0.00)	NA	0.00 (0.00)
FDR-Conformal	5 (3.76)	0.99 (0.01)	NA	0.07 (0.05)
HP-Pointwise	11 (5.49)	0.95 (0.02)	0.82 (0.02)	0.27 (0.09)
HP-Uniform	3 (1.46)	0.97 (0.02)	0.82 (0.02)	0.16 (0.07)
HP-LTT	3 (1.61)	0.97 (0.02)	0.81 (0.02)	0.16 (0.07)
Horizon: 9 months				
Oracle	0 (0.00)	1 (0.00)	NA	0 (0.00)
Model	0 (0.00)	1.00 (0.00)	NA	0.00 (0.00)
FDR-Conformal	0 (0.00)	1.00 (0.00)	NA	0.00 (0.00)
HP-Pointwise	2 (1.13)	0.97 (0.02)	0.77 (0.03)	0.15 (0.07)
HP-Uniform	0 (0.37)	0.99 (0.01)	NA	0.03 (0.03)
HP-LTT	2 (0.81)	0.97 (0.02)	0.76 (0.03)	0.14 (0.07)

Table A2: Detailed numerical summary of results corresponding to Figure 3. Each entry shows the mean and (in parenthesis) two standard errors across repeated trials. Values in bold indicate the method selecting the most patients at each time (among those with valid survival rate). Values highlighted in red denote survival rates significantly below the 90% target.

Method	Yield	Survival	Survival (cond.)	$P(\widehat{\mathcal{S}} > 0)$
Horizon: 2 months				
Oracle	841 (5.12)	1 (0.00)	1 (0.00)	1 (0.00)
Model	859 (7.72)	0.89 (0.00)	0.89 (0.00)	1.00 (0.00)
FDR-Conformal	630 (62.51)	0.90 (0.01)	0.90 (0.00)	0.96 (0.06)
HP-Pointwise	373 (78.16)	0.93 (0.01)	0.92 (0.01)	0.96 (0.06)
HP-Uniform	21 (17.41)	0.98 (0.01)	0.95 (0.01)	0.41 (0.15)
HP-LTT	276 (88.31)	0.95 (0.01)	0.91 (0.01)	0.52 (0.15)
Horizon: 3 months				
Oracle	536 (5.70)	1 (0.00)	1 (0.00)	1 (0.00)
Model	705 (9.55)	0.85 (0.00)	0.85 (0.00)	1.00 (0.00)
FDR-Conformal	157 (44.25)	0.93 (0.02)	0.89 (0.01)	0.67 (0.14)
HP-Pointwise	49 (27.37)	0.97 (0.01)	0.92 (0.01)	0.44 (0.14)
HP-Uniform	6 (3.69)	0.98 (0.01)	0.94 (0.02)	0.31 (0.14)
HP-LTT	8 (11.54)	0.99 (0.01)	NA	0.04 (0.06)
Horizon: 6 months				
Oracle	26 (1.81)	1 (0.02)	1 (0.02)	1 (0.00)
Model	438 (8.81)	0.76 (0.01)	0.76 (0.01)	1.00 (0.00)
FDR-Conformal	4 (3.68)	0.98 (0.02)	0.82 (0.01)	0.10 (0.09)
HP-Pointwise	3 (4.06)	0.98 (0.02)	NA	0.08 (0.08)
HP-Uniform	1 (1.96)	0.98 (0.02)	NA	0.06 (0.07)
HP-LTT	2 (3.43)	1.00 (0.01)	NA	0.02 (0.04)
Horizon: 9 months				
Oracle	0 (0.00)	1 (0.00)	NA	0 (0.00)
Model	304 (7.73)	0.68 (0.01)	0.68 (0.01)	1.00 (0.00)
FDR-Conformal	2 (2.09)	0.98 (0.02)	NA	0.06 (0.07)
HP-Pointwise	1 (1.20)	0.97 (0.03)	NA	0.06 (0.07)
HP-Uniform	0 (0.28)	0.99 (0.02)	NA	0.02 (0.04)
HP-LTT	0 (0.00)	1.00 (0.00)	NA	0.00 (0.00)

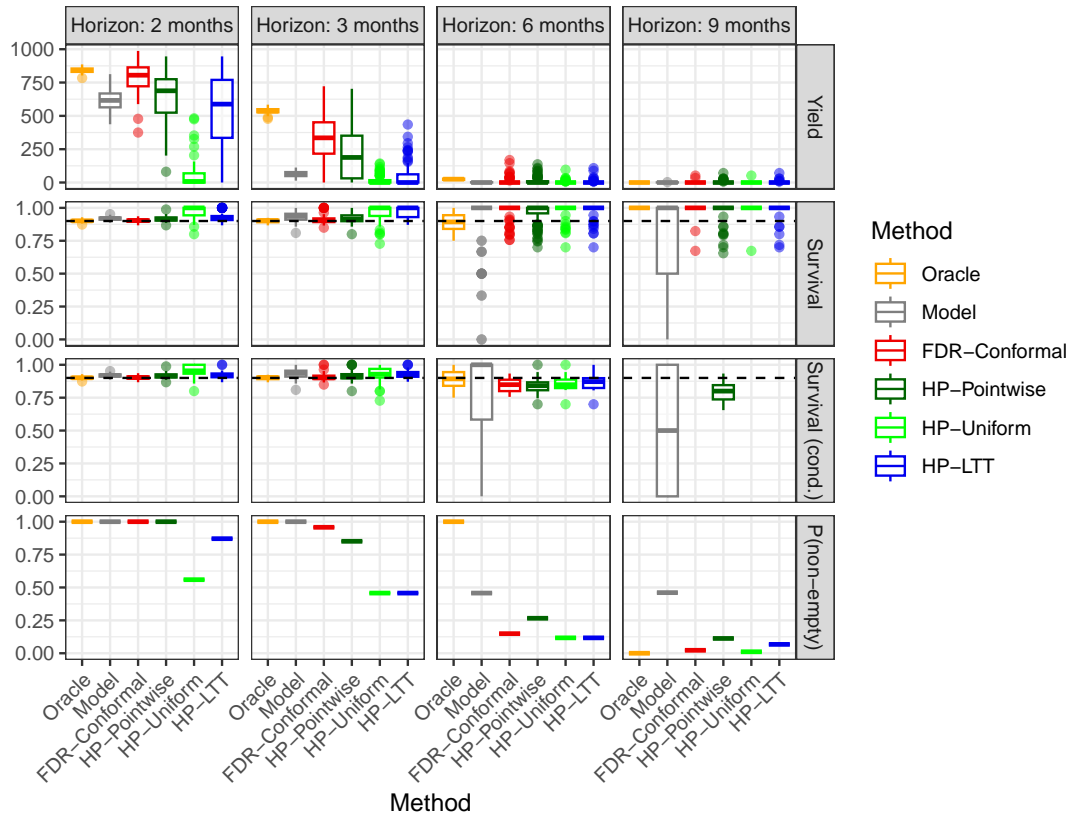


Figure A1: Summary of low-risk screening results obtained by applying different calibration methods to semi-synthetic oncology data simulated using a random forest generative model, at different screening horizons. All methods use the same mis-specified Cox survival model. Other details as in Figure 1.

Table A3: Detailed numerical summary of results corresponding to Figure A1. Each entry shows the mean and (in parenthesis) two standard errors across repeated trials. Values in bold indicate the method selecting the most patients at each time (among those with valid survival rate). Values highlighted in red denote survival rates significantly below the 90% target.

Method	Yield	Survival	Survival (cond.)	$P(\widehat{\mathcal{S}} > 0)$
Horizon: 2 months				
Oracle	841 (3.75)	1 (0.00)	1 (0.00)	1 (0.00)
Model	612 (15.86)	0.92 (0.00)	0.92 (0.00)	1.00 (0.00)
FDR-Conformal	787 (22.40)	0.90 (0.00)	0.90 (0.00)	1.00 (0.00)
HP-Pointwise	636 (37.58)	0.92 (0.00)	0.92 (0.00)	1.00 (0.00)
HP-Uniform	51 (19.69)	0.97 (0.01)	0.95 (0.01)	0.56 (0.10)
HP-LTT	520 (59.32)	0.93 (0.01)	0.92 (0.00)	0.87 (0.07)
Horizon: 3 months				
Oracle	538 (4.28)	1 (0.00)	1 (0.00)	1 (0.00)
Model	63 (4.74)	0.93 (0.01)	0.93 (0.01)	1.00 (0.00)
FDR-Conformal	340 (38.85)	0.91 (0.01)	0.91 (0.01)	0.96 (0.04)
HP-Pointwise	219 (38.70)	0.93 (0.01)	0.91 (0.01)	0.85 (0.07)
HP-Uniform	18 (6.72)	0.97 (0.01)	0.93 (0.01)	0.46 (0.10)
HP-LTT	50 (17.99)	0.97 (0.01)	0.93 (0.01)	0.46 (0.10)
Horizon: 6 months				
Oracle	25 (1.21)	1 (0.01)	1 (0.01)	1 (0.00)
Model	1 (0.28)	0.91 (0.04)	0.81 (0.06)	0.46 (0.10)
FDR-Conformal	9 (5.80)	0.98 (0.01)	0.84 (0.01)	0.15 (0.07)
HP-Pointwise	13 (5.72)	0.96 (0.02)	0.84 (0.01)	0.27 (0.09)
HP-Uniform	3 (2.37)	0.98 (0.01)	0.86 (0.02)	0.12 (0.07)
HP-LTT	4 (3.18)	0.98 (0.01)	0.86 (0.02)	0.12 (0.07)
Horizon: 9 months				
Oracle	0 (0.00)	1 (0.00)	NA	0 (0.00)
Model	1 (0.15)	0.78 (0.08)	0.52 (0.10)	0.46 (0.11)
FDR-Conformal	1 (1.39)	0.99 (0.01)	NA	0.02 (0.03)
HP-Pointwise	3 (2.10)	0.98 (0.02)	0.79 (0.02)	0.11 (0.07)
HP-Uniform	1 (1.17)	1.00 (0.01)	NA	0.01 (0.02)
HP-LTT	2 (1.86)	0.99 (0.01)	NA	0.07 (0.05)

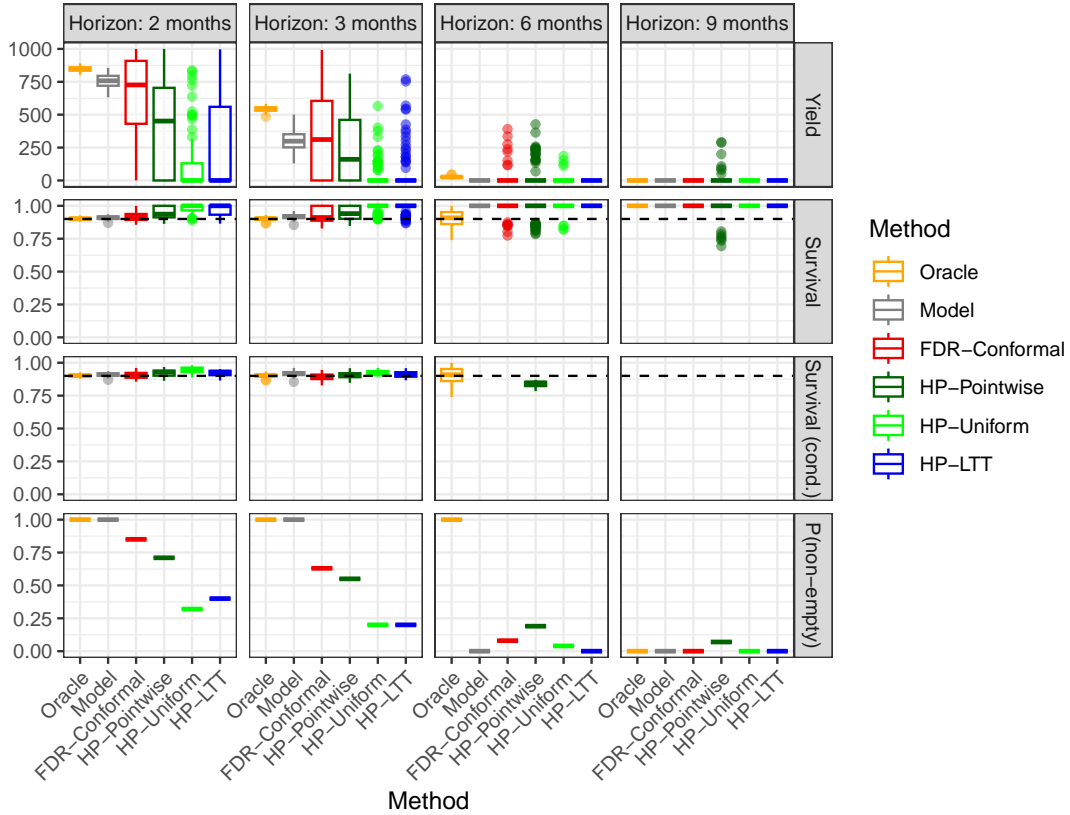


Figure A2: Summary of low-risk screening results obtained by applying different methods to semi-synthetic oncology data simulated from a grf generative survival model, at different screening horizons. Calibration sample size 100. Other details as in Figure 1.

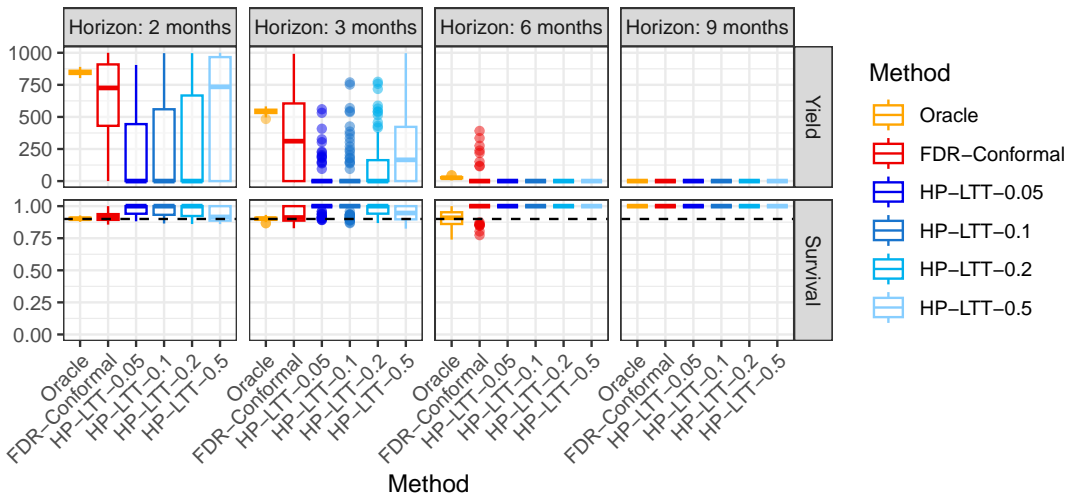


Figure A3: Summary of low-risk screening results on semi-synthetic oncology data, similar to Figure 1. The LTT calibration method is applied at different confidence levels δ , ranging from $\delta = 0.05$ (more conservative) to $\delta = 0.5$ (more liberal). Here, the calibration sample size is 100 instead of 1000.

Table A4: Detailed numerical summary of results corresponding to Figure A2. Each entry shows the mean and (in parenthesis) two standard errors across repeated trials. Values in bold indicate the method selecting the most patients at each time (among those with valid survival rate). Values highlighted in red denote survival rates significantly below the 90% target.

Method	Yield	Survival	Survival (cond.)	$P(\hat{S} > 0)$
Horizon: 2 months				
Oracle	847 (3.54)	1 (0.00)	1 (0.00)	1 (0.00)
Model	758 (10.09)	0.91 (0.00)	0.91 (0.00)	1.00 (0.00)
FDR-Conformal	628 (67.50)	0.92 (0.01)	0.91 (0.00)	0.85 (0.07)
HP-Pointwise	419 (69.35)	0.94 (0.01)	0.92 (0.01)	0.71 (0.09)
HP-Uniform	110 (42.39)	0.98 (0.01)	0.94 (0.00)	0.32 (0.09)
HP-LTT	255 (66.33)	0.97 (0.01)	0.92 (0.00)	0.40 (0.10)
Horizon: 3 months				
Oracle	543 (4.08)	1 (0.00)	1 (0.00)	1 (0.00)
Model	299 (15.23)	0.92 (0.00)	0.92 (0.00)	1.00 (0.00)
FDR-Conformal	329 (62.00)	0.93 (0.01)	0.89 (0.01)	0.63 (0.10)
HP-Pointwise	233 (52.32)	0.95 (0.01)	0.90 (0.01)	0.55 (0.10)
HP-Uniform	40 (19.46)	0.98 (0.01)	0.92 (0.00)	0.20 (0.08)
HP-LTT	68 (32.61)	0.98 (0.01)	0.91 (0.00)	0.20 (0.08)
Horizon: 6 months				
Oracle	26 (1.19)	1 (0.01)	1 (0.01)	1 (0.00)
Model	0 (0.00)	1.00 (0.00)	NA	0.00 (0.00)
FDR-Conformal	18 (13.66)	0.99 (0.01)	NA	0.08 (0.05)
HP-Pointwise	41 (18.31)	0.97 (0.01)	0.84 (0.01)	0.19 (0.08)
HP-Uniform	6 (5.80)	0.99 (0.01)	NA	0.04 (0.04)
HP-LTT	0 (0.00)	1.00 (0.00)	NA	0.00 (0.00)
Horizon: 9 months				
Oracle	0 (0.00)	1 (0.00)	NA	0 (0.00)
Model	0 (0.00)	1.00 (0.00)	NA	0.00 (0.00)
FDR-Conformal	0 (0.00)	1.00 (0.00)	NA	0.00 (0.00)
HP-Pointwise	11 (9.51)	0.98 (0.01)	NA	0.07 (0.05)
HP-Uniform	0 (0.00)	1.00 (0.00)	NA	0.00 (0.00)
HP-LTT	0 (0.00)	1.00 (0.00)	NA	0.00 (0.00)

A3.2 Experiments with Real Data

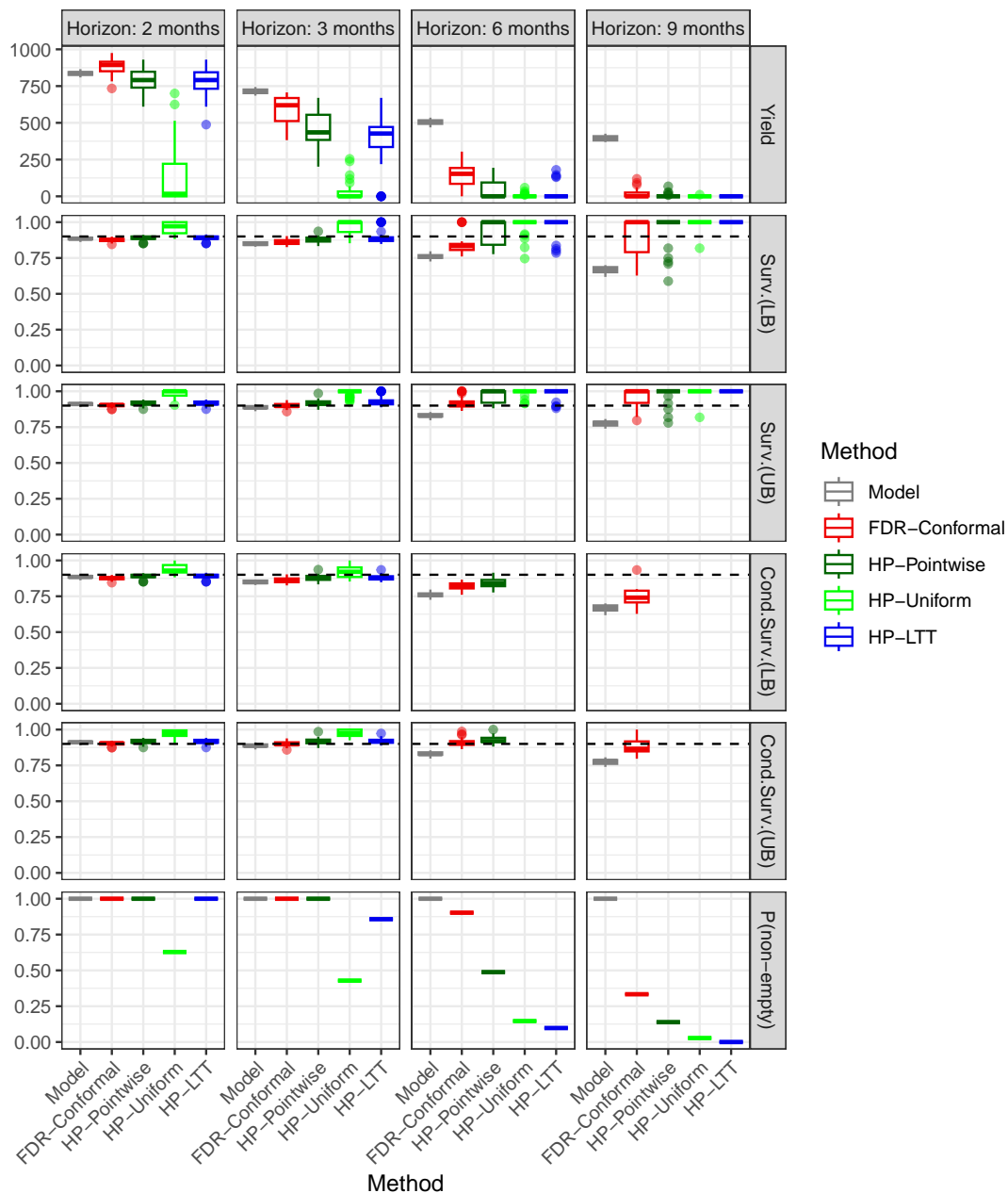


Figure A4: Summary of low-risk screening results obtained by applying different methods to real oncology data, at different screening horizons, using a gradient boosting survival model. Other details as in Table 2.

Table A5: Summary of low-risk screening results obtained by applying different methods to real oncology data, at different screening horizons, using a Cox survival model. Other details are as in Table 2.

Method	Yield	Surv.(LB)	Surv.(UB)	C.Surv.(LB)	C.Surv.(UB)	$P(\hat{S} > 0)$
Horizon: 2 months						
Model	823 (4.21)	0.89 (0.00)	0.92 (0.00)	0.89 (0.00)	0.92 (0.00)	1.00 (0.00)
FDR-Conformal	917 (7.87)	0.87 (0.00)	0.90 (0.00)	0.87 (0.00)	0.90 (0.00)	1.00 (0.00)
HP-Pointwise	860 (11.83)	0.89 (0.00)	0.91 (0.00)	0.89 (0.00)	0.91 (0.00)	1.00 (0.00)
HP-Uniform	186 (65.31)	0.97 (0.01)	0.98 (0.01)	0.93 (0.01)	0.96 (0.01)	0.42 (0.12)
HP-LTT	860 (11.79)	0.89 (0.00)	0.91 (0.00)	0.89 (0.00)	0.91 (0.00)	1.00 (0.00)
Horizon: 3 months						
Model	390 (4.17)	0.91 (0.00)	0.95 (0.00)	0.91 (0.00)	0.95 (0.00)	1.00 (0.00)
FDR-Conformal	682 (13.55)	0.86 (0.00)	0.90 (0.00)	0.86 (0.00)	0.90 (0.00)	1.00 (0.00)
HP-Pointwise	608 (20.18)	0.88 (0.00)	0.91 (0.00)	0.88 (0.00)	0.91 (0.00)	1.00 (0.00)
HP-Uniform	87 (34.33)	0.97 (0.01)	0.98 (0.01)	0.92 (0.01)	0.96 (0.01)	0.42 (0.11)
HP-LTT	583 (28.84)	0.88 (0.01)	0.92 (0.01)	0.88 (0.01)	0.92 (0.01)	1.00 (0.00)
Horizon: 6 months						
Model	32 (1.81)	0.88 (0.01)	0.96 (0.01)	0.88 (0.01)	0.96 (0.01)	1.00 (0.00)
FDR-Conformal	211 (22.79)	0.86 (0.01)	0.92 (0.01)	0.84 (0.01)	0.91 (0.01)	0.91 (0.07)
HP-Pointwise	136 (26.94)	0.90 (0.02)	0.94 (0.01)	0.85 (0.01)	0.92 (0.01)	0.72 (0.10)
HP-Uniform	14 (6.98)	0.97 (0.01)	0.99 (0.01)	0.89 (0.01)	0.95 (0.01)	0.28 (0.10)
HP-LTT	43 (20.46)	0.96 (0.02)	0.98 (0.01)	0.87 (0.01)	0.93 (0.01)	0.32 (0.11)
Horizon: 9 months						
Model	6 (0.85)	0.87 (0.03)	0.97 (0.02)	0.86 (0.03)	0.96 (0.02)	0.92 (0.06)
FDR-Conformal	35 (9.34)	0.88 (0.03)	0.94 (0.01)	0.80 (0.01)	0.90 (0.01)	0.59 (0.11)
HP-Pointwise	21 (8.69)	0.92 (0.02)	0.97 (0.01)	0.80 (0.01)	0.92 (0.01)	0.39 (0.11)
HP-Uniform	3 (2.12)	0.98 (0.01)	0.99 (0.01)	0.82 (0.02)	0.92 (0.01)	0.11 (0.07)
HP-LTT	7 (5.01)	0.96 (0.02)	0.98 (0.01)	0.80 (0.02)	0.93 (0.01)	0.22 (0.10)

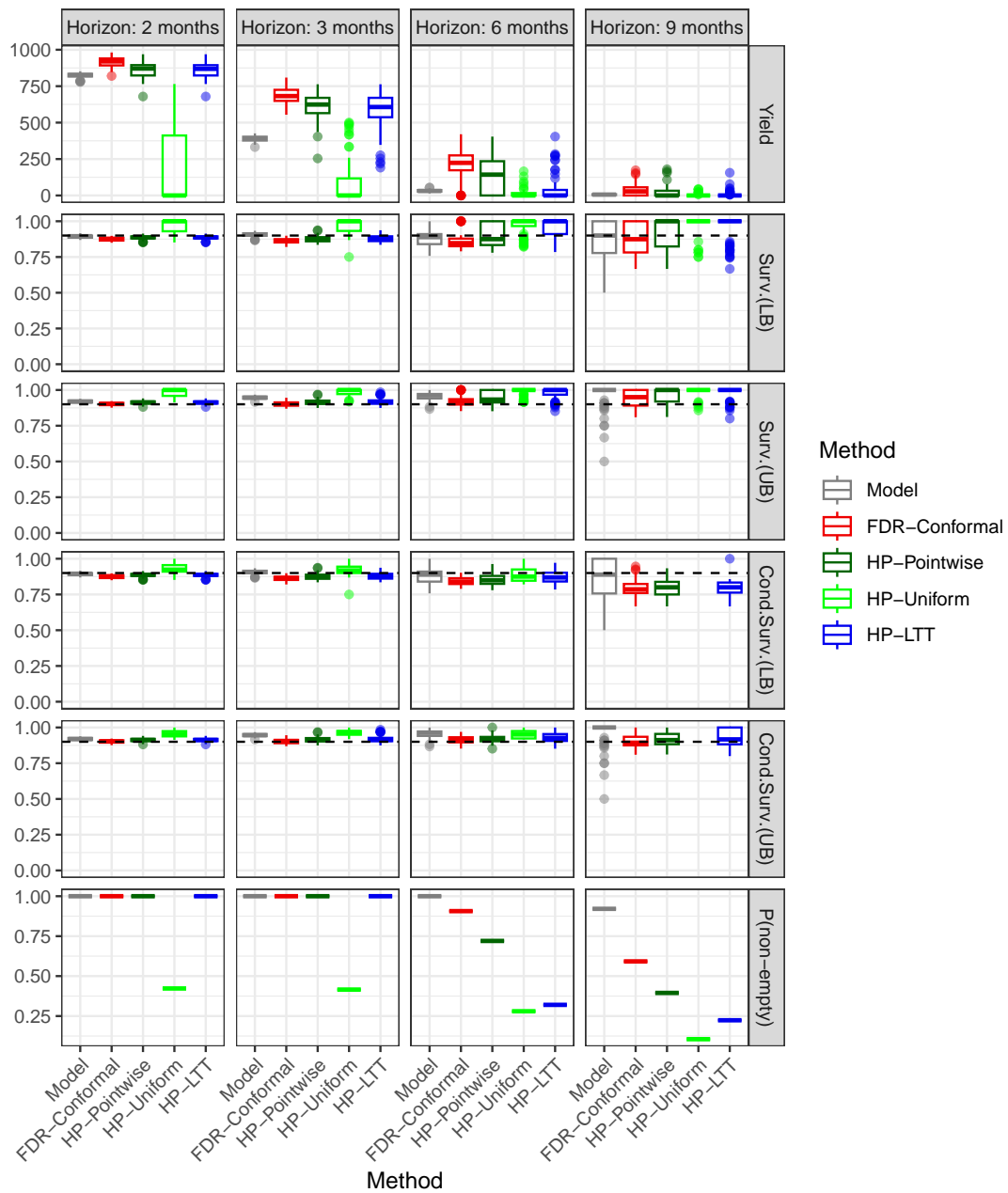


Figure A5: Summary of low-risk screening results obtained by applying different methods to real oncology data, at different screening horizons, using a Cox survival model. Other details as in Figure A4.

Table A6: Summary of low-risk screening results obtained by applying different methods to real oncology data, at different screening horizons, using a generalized random forest survival model. Other details are as in Table 2.

Method	Yield	Surv.(LB)	Surv.(UB)	C.Surv.(LB)	C.Surv.(UB)	$P(\hat{S} > 0)$
Horizon: 2 months						
Model	834 (4.43)	0.89 (0.00)	0.92 (0.00)	0.89 (0.00)	0.92 (0.00)	1.00 (0.00)
FDR-Conformal	868 (11.11)	0.88 (0.00)	0.91 (0.00)	0.88 (0.00)	0.91 (0.00)	1.00 (0.00)
HP-Pointwise	840 (13.93)	0.89 (0.00)	0.91 (0.00)	0.89 (0.00)	0.91 (0.00)	1.00 (0.00)
HP-Uniform	351 (61.33)	0.95 (0.01)	0.96 (0.01)	0.93 (0.01)	0.95 (0.00)	0.72 (0.09)
HP-LTT	838 (14.75)	0.89 (0.00)	0.91 (0.00)	0.89 (0.00)	0.91 (0.00)	1.00 (0.00)
Horizon: 3 months						
Model	509 (4.56)	0.89 (0.00)	0.92 (0.00)	0.89 (0.00)	0.92 (0.00)	1.00 (0.00)
FDR-Conformal	603 (18.39)	0.87 (0.00)	0.91 (0.00)	0.87 (0.00)	0.91 (0.00)	1.00 (0.00)
HP-Pointwise	560 (21.41)	0.88 (0.00)	0.92 (0.00)	0.88 (0.00)	0.92 (0.00)	1.00 (0.00)
HP-Uniform	160 (34.52)	0.95 (0.01)	0.97 (0.01)	0.92 (0.01)	0.96 (0.01)	0.71 (0.09)
HP-LTT	538 (26.77)	0.88 (0.01)	0.92 (0.00)	0.88 (0.01)	0.92 (0.00)	0.99 (0.02)
Horizon: 6 months						
Model	13 (1.31)	0.93 (0.02)	0.98 (0.01)	0.93 (0.02)	0.98 (0.01)	1.00 (0.00)
FDR-Conformal	82 (18.14)	0.91 (0.02)	0.95 (0.01)	0.85 (0.01)	0.92 (0.01)	0.60 (0.10)
HP-Pointwise	130 (18.48)	0.88 (0.01)	0.94 (0.01)	0.87 (0.01)	0.93 (0.01)	0.92 (0.06)
HP-Uniform	19 (7.91)	0.96 (0.01)	0.98 (0.01)	0.90 (0.01)	0.95 (0.01)	0.37 (0.10)
HP-LTT	33 (15.38)	0.96 (0.01)	0.98 (0.01)	0.89 (0.01)	0.94 (0.01)	0.36 (0.10)
Horizon: 9 months						
Model	0 (0.00)	1.00 (0.00)	1.00 (0.00)	NA	NA	0.00 (0.00)
FDR-Conformal	2 (2.19)	0.99 (0.01)	1.00 (0.00)	NA	NA	0.04 (0.04)
HP-Pointwise	28 (8.51)	0.92 (0.02)	0.95 (0.01)	0.81 (0.01)	0.90 (0.01)	0.43 (0.10)
HP-Uniform	3 (2.18)	0.98 (0.01)	0.99 (0.01)	0.82 (0.02)	0.92 (0.01)	0.13 (0.07)
HP-LTT	6 (3.52)	0.97 (0.01)	0.98 (0.01)	0.83 (0.01)	0.90 (0.01)	0.19 (0.08)

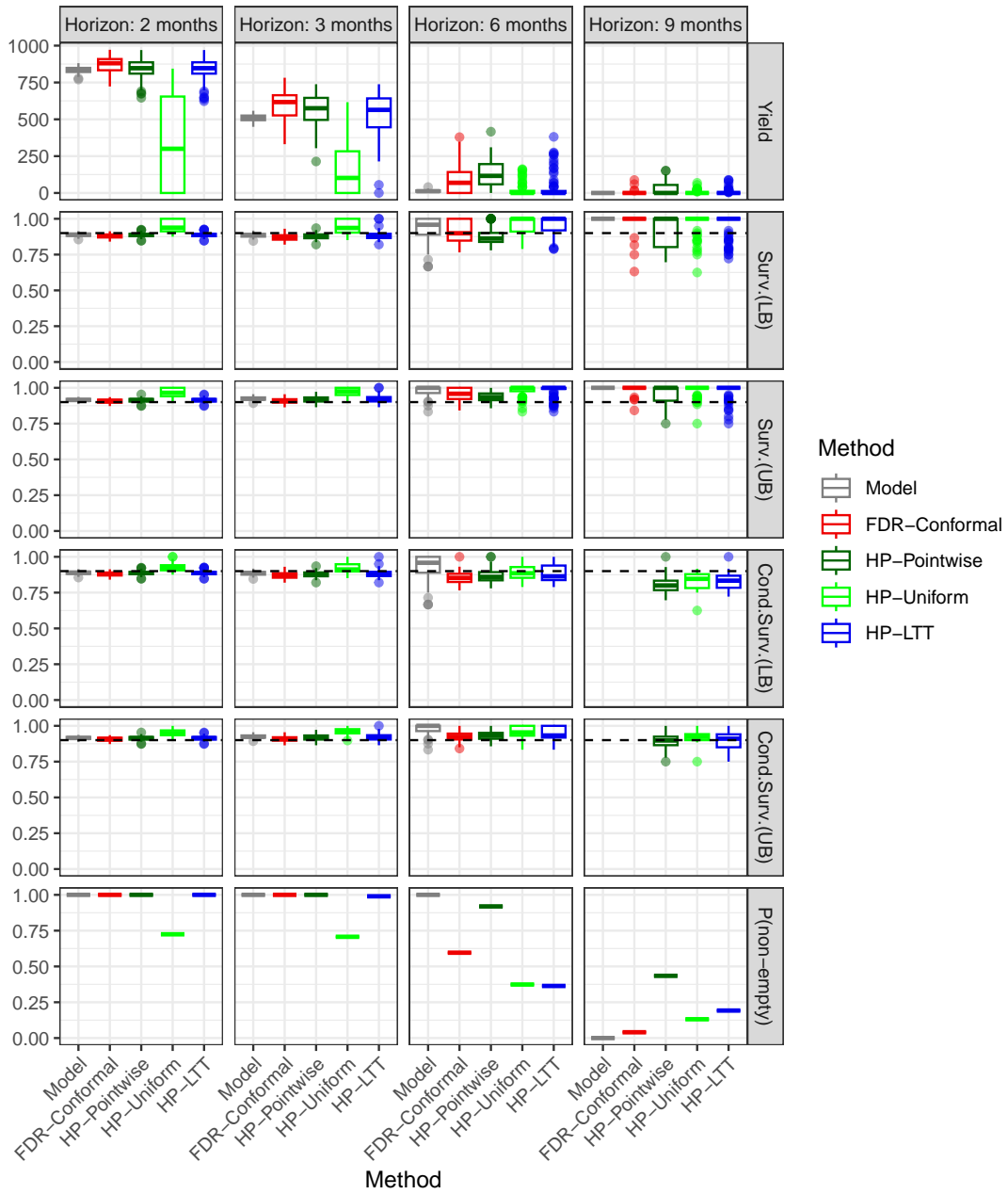


Figure A6: Summary of low-risk screening results obtained by applying different methods to real oncology data, at different screening horizons, using a generalized random forest survival model. Other details as in Figure A4.

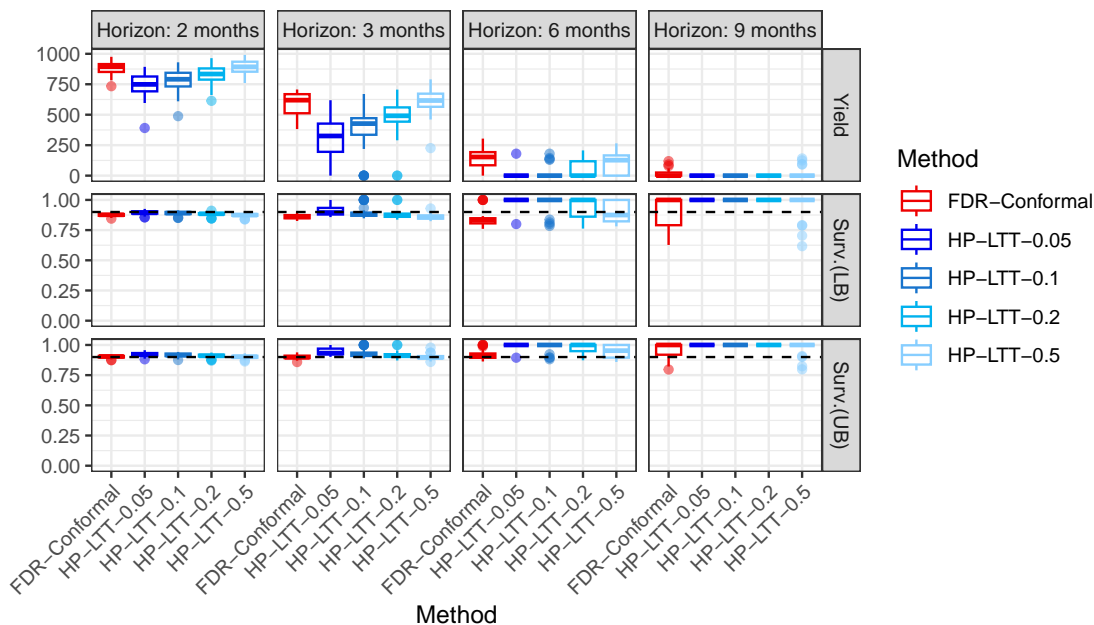


Figure A7: Summary of low-risk screening results on real oncology data, using a gradient boosting survival model as in Figure A4. Here, the LTT calibration method is applied at different confidence levels δ , ranging from $\delta = 0.05$ (more conservative) to $\delta = 0.5$ (more liberal).

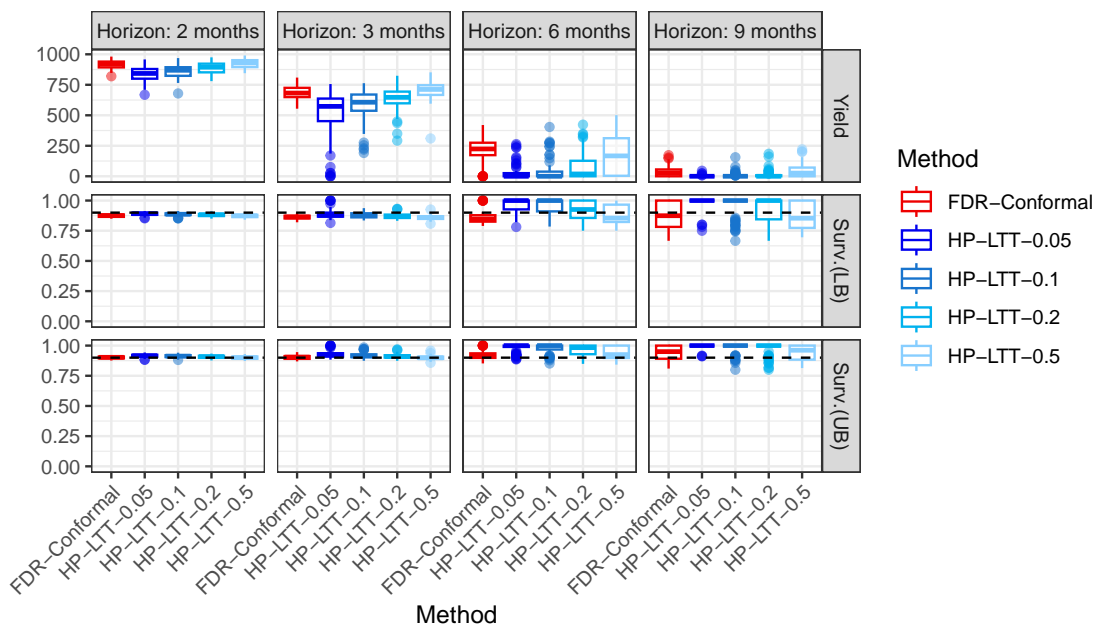


Figure A8: Summary of low-risk screening results on real oncology data, using a Cox survival model as in Figure A5. Here, the LTT calibration method is applied at different confidence levels δ , ranging from $\delta = 0.05$ (more conservative) to $\delta = 0.5$ (more liberal).

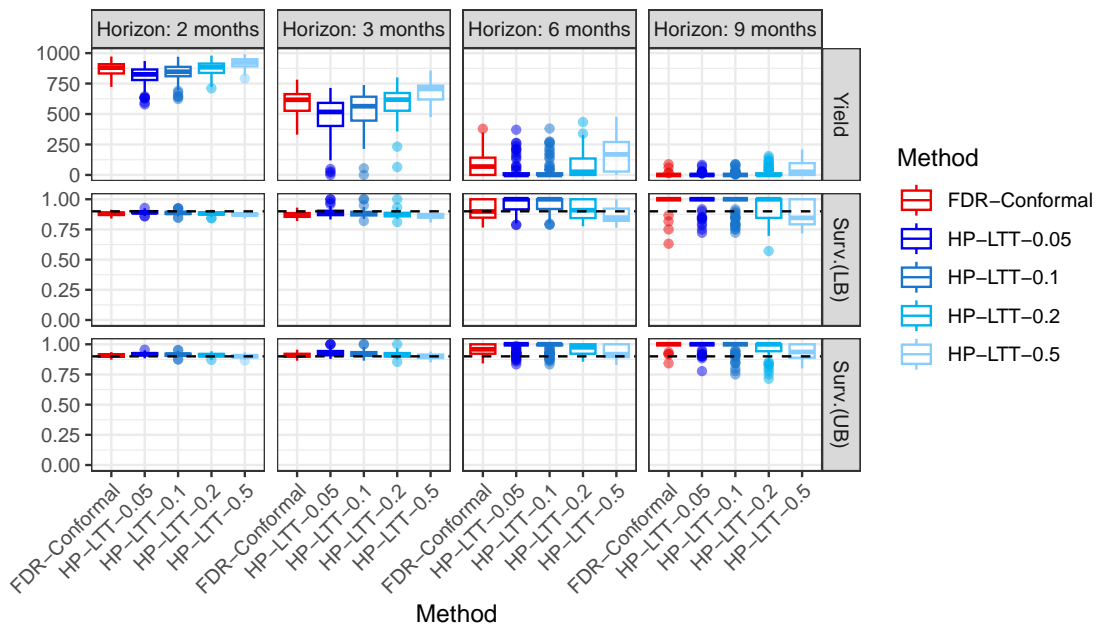


Figure A9: Summary of low-risk screening results on real oncology data, using a generalized random forest survival model as in Figure A6. Here, the LTT calibration method is applied at different confidence levels δ , ranging from $\delta = 0.05$ (more conservative) to $\delta = 0.5$ (more liberal).